Active inversion tectonics, simple shear folding and back-thrusting at Rioni Basin, Georgia

A. Tibaldi[1)], V. Alania[2)], F. L. Bonali[1)], O. Enukidze[2)], N. Tsereteli[2)], N. Kvavadze[2)], O. Varazanashvili[2)]

[1)] *University of Milan Bicocca, Milan, Italy*
[2)] *M. Nodia Institute of Geophysics, M. Javakhishvili Tbilisi State University, Georgia*

Abstract

The Rioni Basin, located between the Greater and Lesser Caucasus in Georgia, is an outstanding example of ongoing inversion tectonics. Marine and continental deposits of Cretaceous-Neogene age have been locally uplifted since the ending of Miocene. The area of uplift is of 1300 km^2, and Plio-Quaternary river deposits have been raised up to 200 m above the surrounding plane. Inversion tectonics has been accompanied by the development of south-vergent asymmetrical folds and strike-slip faults along the border of the uplifted area. The folds have locally an en-échelon geometry and microtectonic data indicate rotation of the paleostress direction with time, suggesting simple shear deformation. In the interior of the uplifted area, there are gentle symmetrical folds and one main active south-dipping reverse fault, corresponding to a backthrust. A series of morphostructural clues, the tilting of Quaternary strata, the offset of Quaternary alluvial deposits, and the presence of crustal seismic activity, indicate that compressional tectonics is still active. The combination of field data with seismic reflection sections shows that the inversion tectonics took place through a series of north-dipping blind thrusts and a wedge with passive back-thrusting. Uplift and contraction are more developed along the eastern part of the study area, suggesting the westward propagation of the closure of the Transcaucasian depression.

Key words: Caucasus, active faults, simple shear folds, seismicity, inversion tectonics, backthrusts

1 Introduction

The Caucasus is a young orogenic system that started to develop following the Tertiary collision between the Arabian and Eurasian plates. This collision caused the partial closure of previous basins whose modern remnants are represented by the Black Sea and the Caspian Sea (Fig. 1). Between these two depressions there are the Greater and Lesser Caucasus, separated by the Transcaucasian intermontane valley. In the Transcaucasian depression, during Oligocene-Early Miocene times the Rioni Basin and the Kura Basin developed as foreland depressions, and successively were involved into the orogenic fold-and-thrust belts (Adamia et al., 1977, 2010, 2011a, 2011b; Banks et al., 1997; Mosar et al., 2010; Sosson et al., 2010, 2013; Forte et al., 2010; Alamia et al., 2016).

The recent geodynamic processes are also testified by the magmatic activity, with volcanoes emplaced both at the edge of the Greater Caucasus, as the Mt Elbrus, or along the Lesser Caucasus (Rebai et al., 1993). The volcanism in the mountain belt, associated to the Eurasian and Arabian plates collision started only in the late Miocene in the central part of the Caucasus (Adamia et al., 1977, 2015; Koronovskii and Demina, 1999).

Recent GPS data and plate tectonic models indicate that, also at nowadays, the Greater and Lesser Caucasus are tectonically very active, with ongoing mountain building processes comprising complex plate boundary interactions with vertical and horizontal strain partitioning (Rebai et al., 1993; Koçyiğit et al., 2001; Reilinger et al., 2006; Tan and Taymaz, 2006; Kadirov et al., 2013). Very active ongoing process of mountain building are also demonstrated by diffuse seismicity with compressional events of magnitude up to 7 (Tsereteli et al., 2016).

All these data indicate that the Caucasus orogens and the Transcaucasus depression represent outstanding examples of recent mountain building processes of Neogene-Quaternary times. The Neogene compression produced partial closure of the Eastern Black Sea and the consequent flexure of its northern margin (Banks et al., 1997). This flexuring, in turn, induced the formation of the relatively small Rioni Basin, which is normally interpreted as a foreland basin filled with late Miocene to Quaternary sediments. In spite of this structural setting, the Rioni Basin also shows a series of folds that suggest inversion tectonics. We thus embarked in a major effort to understand the age and modality of occurrence of this inversion tectonics, also in view of the potential associated seismic hazard in case of still-ongoing processes. The region, in fact, hosts several villages and small towns and an important hydroelectric infrastructure. We thus integrated new field geological-structural, microtectonic and geomorphological data with seismological data and seismic reflection sections, in order to describe the structural architecture of the Rioni Basin. Regional observations have been integrated with detailed and systematic microtectonic data with the aim of understanding the development of the shallow folds and of reconstructing the evolution of stress orientations. The results show that the uplifting Rioni Basin is mostly bounded by south-vergent hidden thrusts, whereas to the east is limited at the surface by simple shear folds. The interior of the uplifting area is affected by a main active backthrust in response to a tectonic wedge. The data here exposed are useful not only for a better comprehension of the structural architecture and seismic hazard of the area, but also as a general example of how active blind thrusts and shallow faults may influence surface structures and landforms.

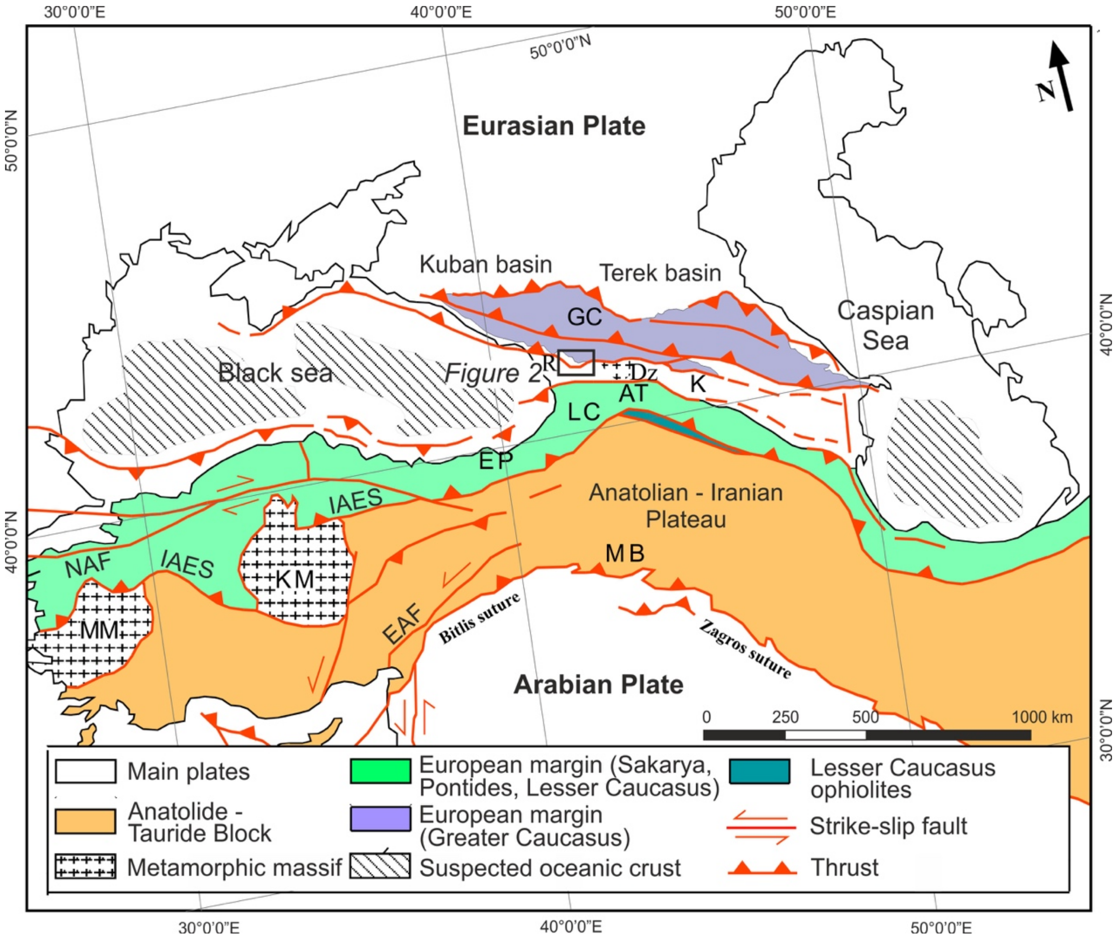

Figure 1. *Tectonic map of the Arabia - Eurasia collision zone (modified from Sosson et al., 2010). Abbreviations: GC-Greater Caucasus; LC-Lesser Caucasus; AT-Achara-Trialeti; R-Rioni; Dz-Dzirula; K-Kura; MB-Mus Basin; EP-Eastern Pontides; KM-Kirsehir Massif; EAF-Eastern Anatolian Fault; NAF-North Anatolian Fault; IAES-Izmir-Ankara-Erzincan Suture; MM-Menderes Massif.*

2 Geological settings

2.1 Regional geology

Rioni Basin is located between the western Greater Caucasus orogen and the Achara-Trialeti fold and thrust belt, which belongs to the northern part of Lesser Caucasus (Fig. 1). The western Greater Caucasus is predominantly a single-vergent orogeny (i.e. southward), in contrast to the central and eastern parts of Greater Caucasus that show a double-vergent orogenic wedge (Forte et al., 2014). During the long Neotethys subduction process, several domains formed in back-arc positions within the Eurasian Plate, mainly the Greater Caucasus basin that opened in Early–Middle Jurassic (Khain, 1974; Dercourt et al., 1986; Adamia et al., 1981, 2011a), and the western and eastern Black Sea basins that opened during the Cretaceous and Cenozoic (Adamia et al., 1974, 1981; Letouzey et al., 1977; Finetti et al., 1988; Zonenshain and Le Pichon, 1986; Okay et al., 1994, 2013; Robinson et al., 1996; Spadini et al., 1996; Cloetingh et al., 2003; Vincent et al., 2005; Yegorova and Gobarenko, 2010; Khriachtchevskaia et al., 2010; Stephenson and Schellart, 2010) or Middle Jurassic-Early Cretaceous (Sosson et al., 2016). Based on apatite fission-track data, the exhumation process in the Greater Caucasus started in the Oligocene and reached the highest rate in the Miocene-Pliocene (Vincent et al., 2007; Vincent et al., 2010; Avdeev and Niemi, 2011). Plate reorganization occurred within the Arabia-Eurasia collision zone at ~5 Ma BP, and first-order plate motions have remained relatively constant since that time (Westaway, 1994; McQuarrie et al. 2003; Allen et al., 2004). The period ~3-5 Ma coincides with the formation of the Zagros fold and thrust belt, South Caspian Sea and Rioni-Kura foreland fold and thrust belts (Adamia et al., 2010; Adamia et al., 2011a; Forte et al., 2010; Devlin et al., 1999). The Apatite fission-track data from the central part of Achara-Trialeti fold and thrust belt (Borjomi area) indicate that exhumation of Paleogene strata and compressional deformation started in Middle Miocene (Albino et al., 2014). According to GPS data, convergence rate between the Greater Caucasus and Lesser Caucasus increases from West to East in the Caucasus region; namely, convergence rate in the Rioni basin is about 4 mm/yr, and in Kura foreland (in Azerbaijan) is about 14 mm/yr (Reilinger et al., 2006).

Rioni Basin developed mainly during the Oligocene-Miocene through loading by the Achara-Trialeti and Greater Caucasus fold and thrust belts (Banks et al., 1997). The northern part of Rioni foreland is characterized by thrusts with a curved geometry in plan view, and is dominated by a thin-skinned tectonic style (Banks et al., 1997;

Adamia et al., 2010, 2011b). Ramp anticlines formed above south-vergent thrusts that detach and flatten along the Upper Jurassic evaporites of the Rioni foreland basin. The anticlines involve Cretaceous-Neogene strata and are arranged en-échelon. These structures are clearly related to compression in the Greater Caucasus (Banks et al., 1997; Adamia et al., 2010). Regionally, the Greater Caucasus frontal folds began to form as early as Late Eocene but anticlines from the northern part of Rioni Basin apparently formed from the Middle Miocene onwards with most growth probably during the Meotian and very little during the Pontian-Recent (Banks et al., 1997). Beneath the ramp anticlines and a similar offshore structure, known as Shatsky Ridge, it can be seen that the top Cretaceous regional surface actually falls by seismic profile across the compressional faults. This suggests that the thrusts overlie earlier extensional faults that are likely to be related to the opening of the Eastern Black Sea. As a consequence, these normal faults should have a Late Paleocene to Early Eocene age (Robinson et al., 1996; Banks et al., 1997).

The frontal folds of the Achara-Trialeti fold and thrust belt form the oil-bearing structures on the southern flank of the Rioni basin. These structures are compressional ramp anticlines formed initially from the Early Sarmatian to the Pontian with minor growth continuing into the Quaternary (Banks et al., 1997; Adamia et al., 2010).

2.2 Stratigraphy of Rioni Basin

The distribution of the main stratigraphic units of Rioni Basin is represented in the geological map of Figure 2 and schematized in the stratigraphic column of Figure 3. The sedimentary cover of the Rioni basin is commonly > 5 km thick (Adamia et al. 2011a). The oldest formation exposed north (Greater Caucasus) of Rioni Basin is represented by Lower Jurassic (about 1500 m thick) sandstones and shales. Pre-Jurassic basement crops out in the Dzirula Massif that separates the Rioni and Kura basins. The Dzirula massif is dominated by pre-Variscan diorite-plagiogneiss-migmatite complex and Variscan granitoids (Zakariadze et al., 2007; Adamia et al., 2011a). The Middle Jurassic deposits are represented by Bajocian tuff-turbidities with rare bands of calk-alkaline andesite-basalts and the Bathonian freshwater-lacustrine coal-bearing sandy-argillaceous rocks; thickness is about 2500 m. The Upper Jurassic rocks are made of evaporites, clastic deposits, and basalts (about 500 m thick). Lower Cretaceous turbidities, dolomites, limestones (Urgonian facies), organogenic limestones and marls, and conglomerates at the base, transgressively rest on the

Upper Jurassic rocks; thickness is about 350-400 m (Adamia et al. 2011a). Within the Rioni Basin and in the surrounding area, there are also Upper Cretaceous, Paleocene and Eocene deposits mainly made of neritic organogenic limestones, marls and volcanogenic rocks; their thickness in some places exceeds 2000 m (Adamia et al. 2011a). The Oligocene-Lower Miocene (Maykopian) series is represented mainly by alternation of gypsiferous clays with sandstones that are highly specific for the Eastern Paratethys; thickness is about 800-900 m (Banks et al., 1997; Jones & Simmons, 1997; Adamia et al., 2010).

Syntectonic strata of Middle - Upper Miocene (Sarmatian and Meotian-Pontian), Pliocene (Cimmerian and Kuyalnikian) and Pleistocene (Gurian) are represented by shallow marine and continental, predominantly terrigenic clastic deposits, conglomerates, sandstones, mudstones, claystones, sandy clays, clays and rare shell-beds. Total thickness of the syntectonic strata is about 1500-2000 m (Banks et al., 1997; Adamia et al., 2010).

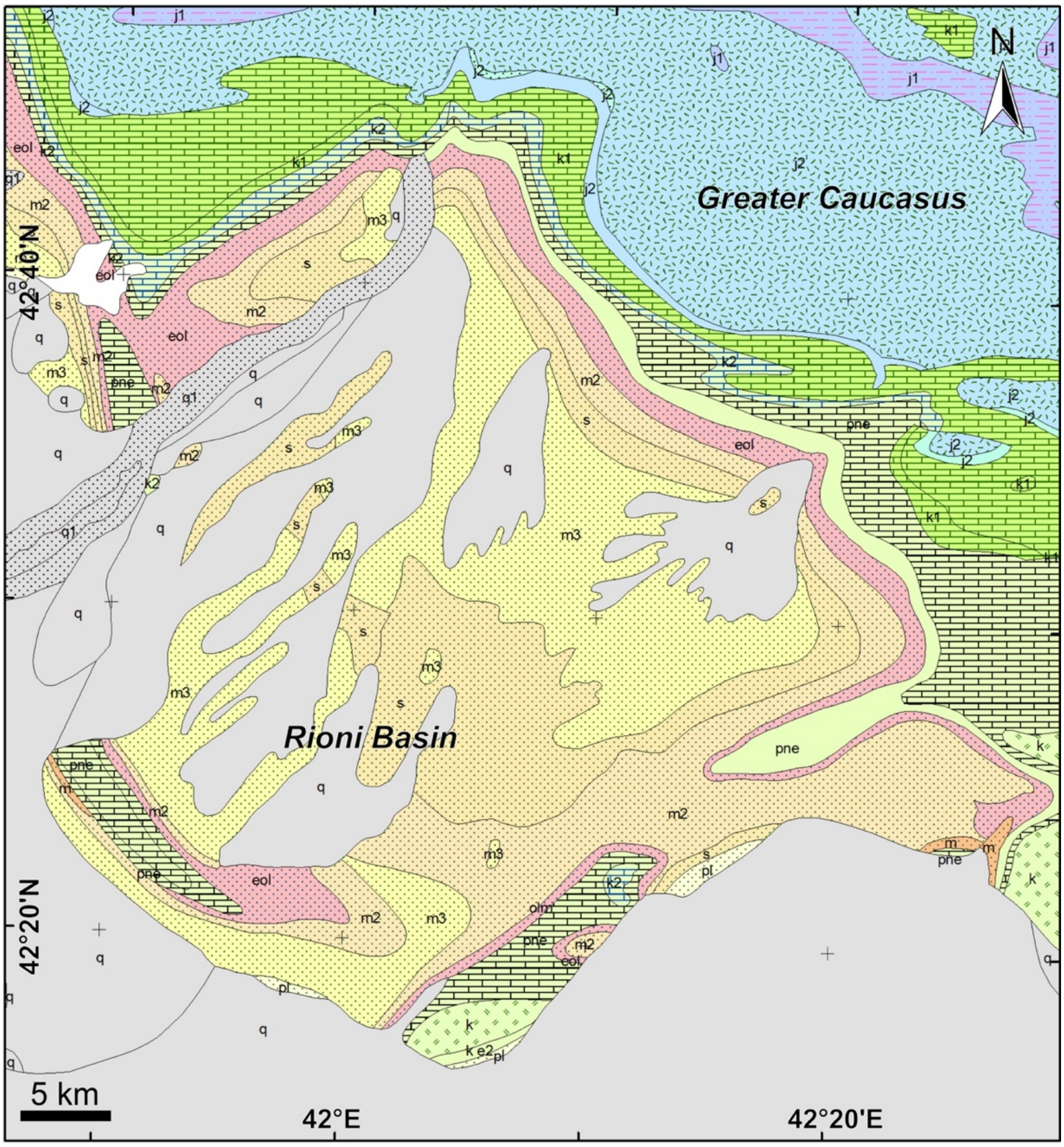

Figure 2. *Geological map of the study area (modified after Adamia and Gujabidze, 2004).*

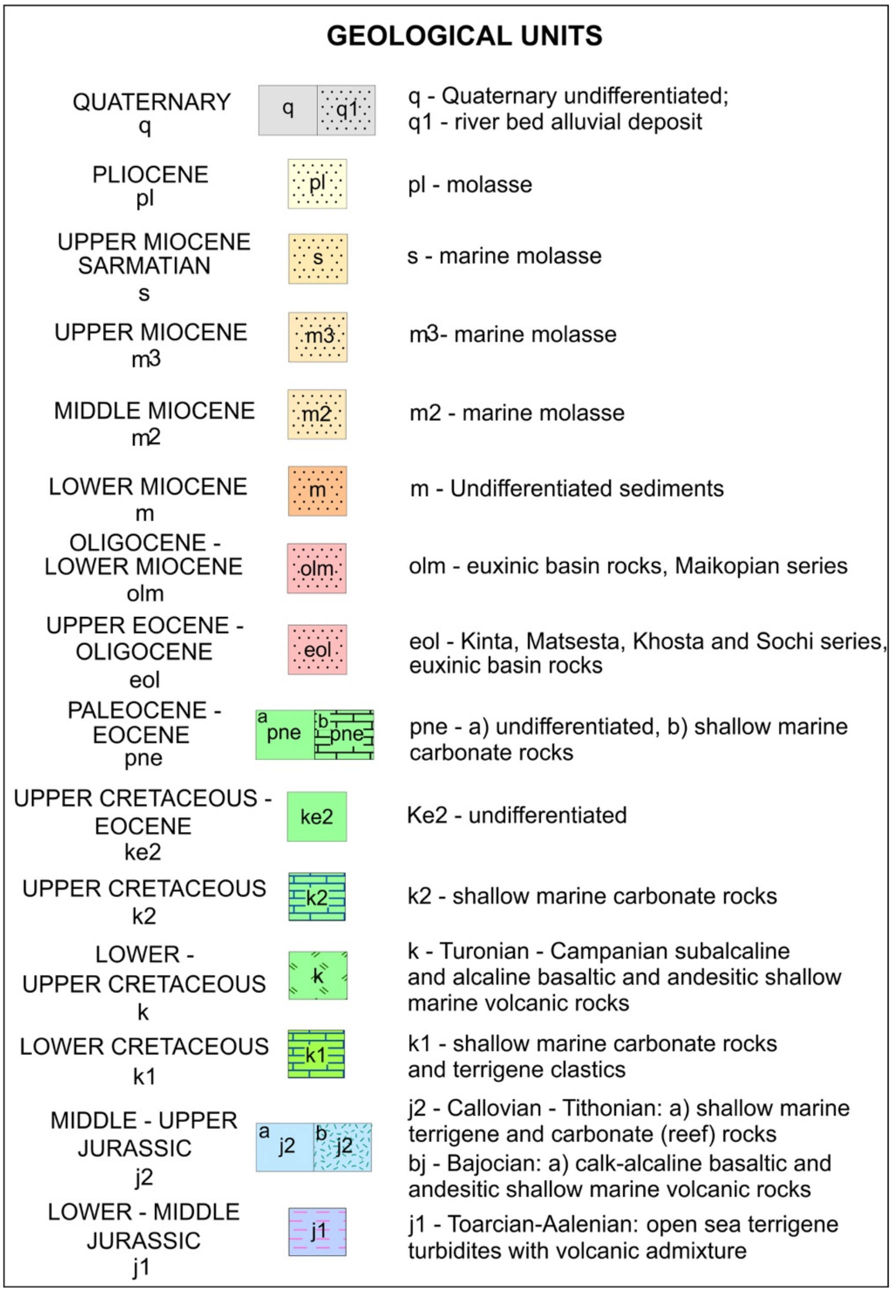

Figure 3. *Lithostratigraphic units present in the Rioni basin and their ages (modified after Adamia and Gujabidze, 2004).*

3 New data

In the next sections we describe the results of a series of multidisciplinary analyses that we carried out in the region. We will describe first the geomorphological observations, then field geological-structural data, seismological data, and seismic reflection profiles.

3.1 Geomorphology

Part of the Rioni Basin presents a series of geomorphological characteristics that deserve attention. While along the coast of Black Sea and towards the Lesser Caucasus, the floor of the Rioni Basin is flat (altitudes mostly < 10 m a.s.l.), more to the north, in the area shown in Figure 4, the topography rises up to 300-400 m a.s.l.

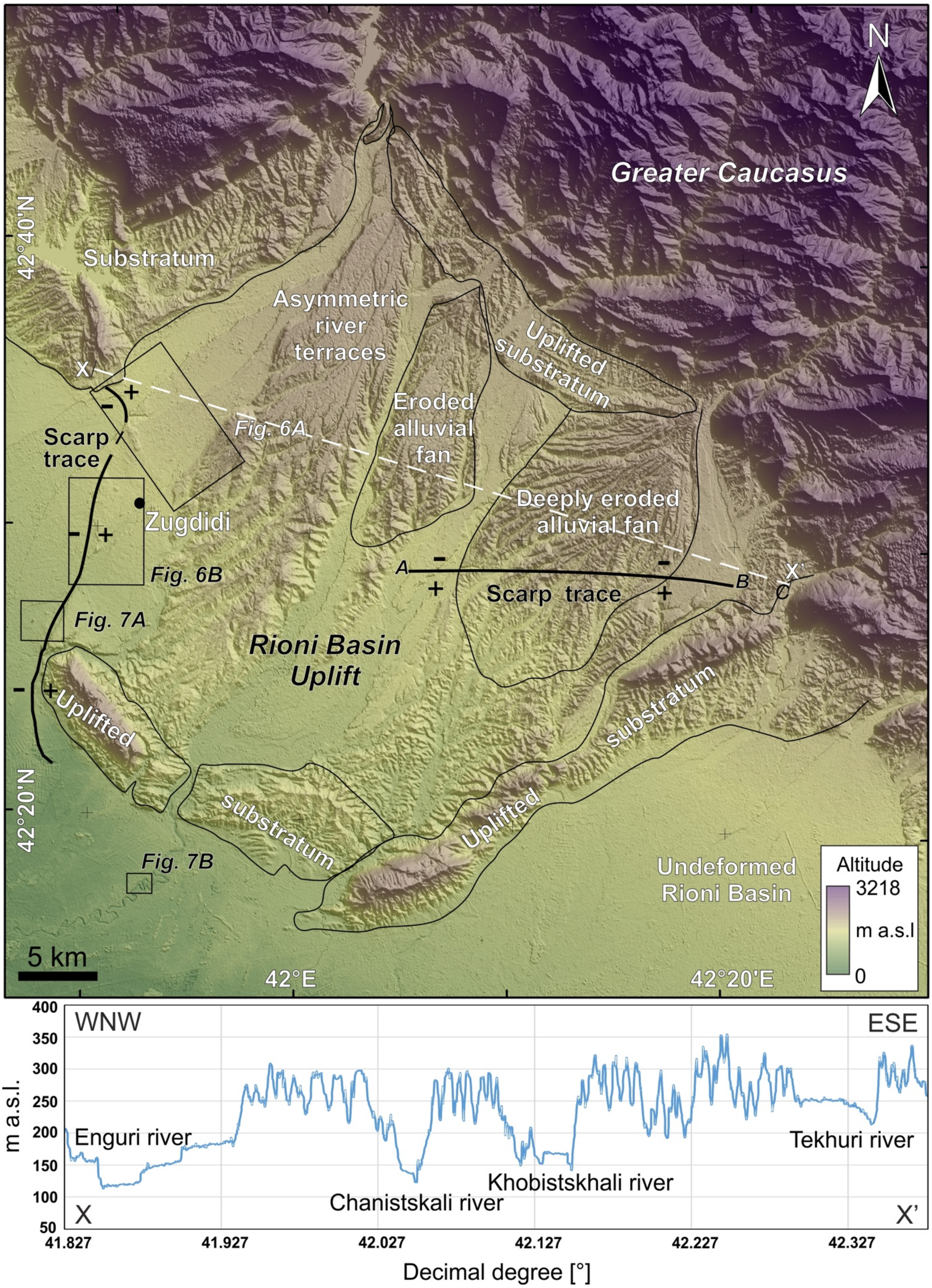

Figure 4. *Digital Elevation Model of Rioni Basin uplift area, with indication of the main geomorphological features and location of Figures 6-7. The graph illustrates the eastward increase of topography along the trace X-X'.*

This area is characterised by a complex morphology with deeply dissected alluvial fans and series of rivers terraces at different altitudes. Elongated features are also present and corresponds to anticline structures as will be described in the chapter dedicated to structural geology.

Most of this relatively high area is covered by fluvial conglomerates of Pliocene-Quaternary age. These conglomerates have been found up to altitudes of 350-400 m (Figs. 5A-B) and thus stand 100-200 m above the surrounding valley floor. The conglomerate succession is in turn deeply incised by the modern Enguri river: for example, at the foothill of the Greater Caucasus, immediately south of the Enguri dam, the river is deeply entrenched in a canyon, with the river bed located at 305-290 m a.s.l. (Fig. 5A) This canyon has been cut into the carbonatic bedrock, leaving a river terrace with conglomerates at an altitude of 409-395 m a.s.l. Another parallel river, located more to the east, also excavated a 140-600 m deep gorge into the same bedrock. More to the south, the northern segment of the Enguri river flows at an altitude of 255-240 m a.s.l.; along the same course segment, the conglomerates in the upper terraces stand up to 370 m a.s.l., indicating an erosion of about 120 m. At the foothill of the Greater Caucasus there are also two large alluvial fans (Fig. 4). They show deep river incisions and are in turn cut by more recent terraces, especially to the west.

The river terraces are particularly developed along the Enguri valley, in the western part of this high area. Most, if not all of them, are asymmetric terraces, in the sense that they developed only on the eastern side of the river valley. As an example, we can see in Figure 6A the strong asymmetry of the river terraces produced by the Enguri river. In the background of this oblique view of the area (looking north), it is possible to observe that at least eight orders of river terraces are present on the eastern side of the Enguri river, suggesting a gradual migration of the river in the opposite direction. The bottom of this series of river beds is interrupted along the zone A-B-C (Fig. 6A) by a slight uplifted topography elongated NNW-SSE, and standing from a few meters up to 20 m respect to the valley floor further south. This uplifted zone is transversal to the modern course of the Enguri river, and the latter is obliged to make a deviation towards SE. Part of the river is capable of flowing again towards south at point B, but the zone of uplift deflected part of the water course more to the SE, allowing southward flow of the river only at point C.

The above described morphological scarp can be followed more to the south, at the western side of the town of Zugdidi and further south (see the complete trace in Fig. 4). Near Zugdidi in fact (Fig. 6B), there is a N-S-striking escarpment, facing westwards, about 10-35 m high respect to the valley floor further west. This feature can resemble a river terrace escarpment, but detailed measurement of the topography along the foot and the upper edge of the scarp, shows that altitudes slightly increase southwards. If this escarpment was a river terrace, it should have had a slight decrease in altitude in the direction of river flow, which is to say southward. The fact instead that the altitude increases in that direction, suggests that this escarpment might represent a tectonic

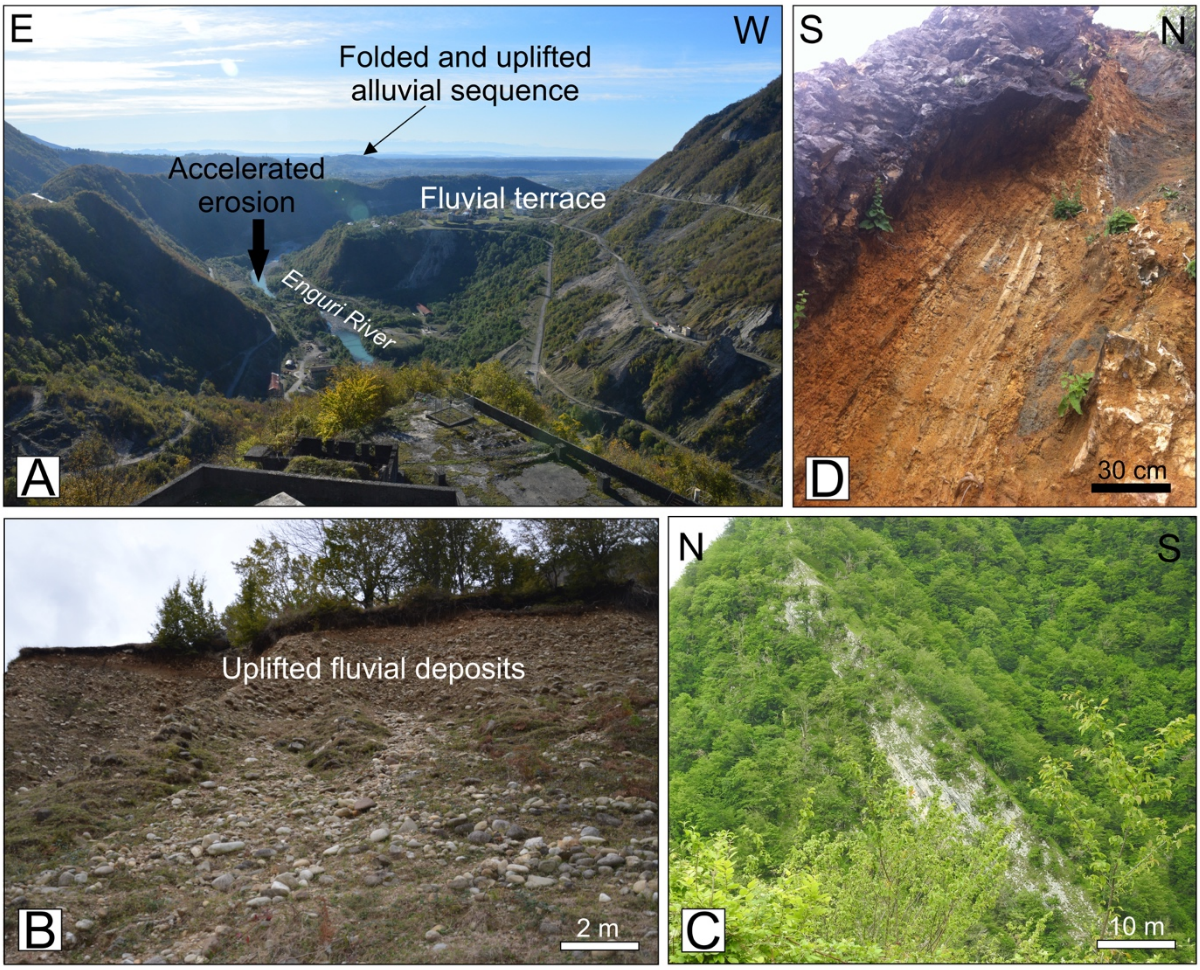

Figure 5. *(A) River terraces and (B) fluvial conglomerates standing up to altitudes of 150-200 m respect to the present valley floor. (C) Near Enguri, the substrate of carbonatic rocks of the Greater Caucasus shows a dominant dip towards S forming a steep monocline. (D) The southern limb of the Senaki fold shows steeply-dipping volcanic and sedimentary strata.*

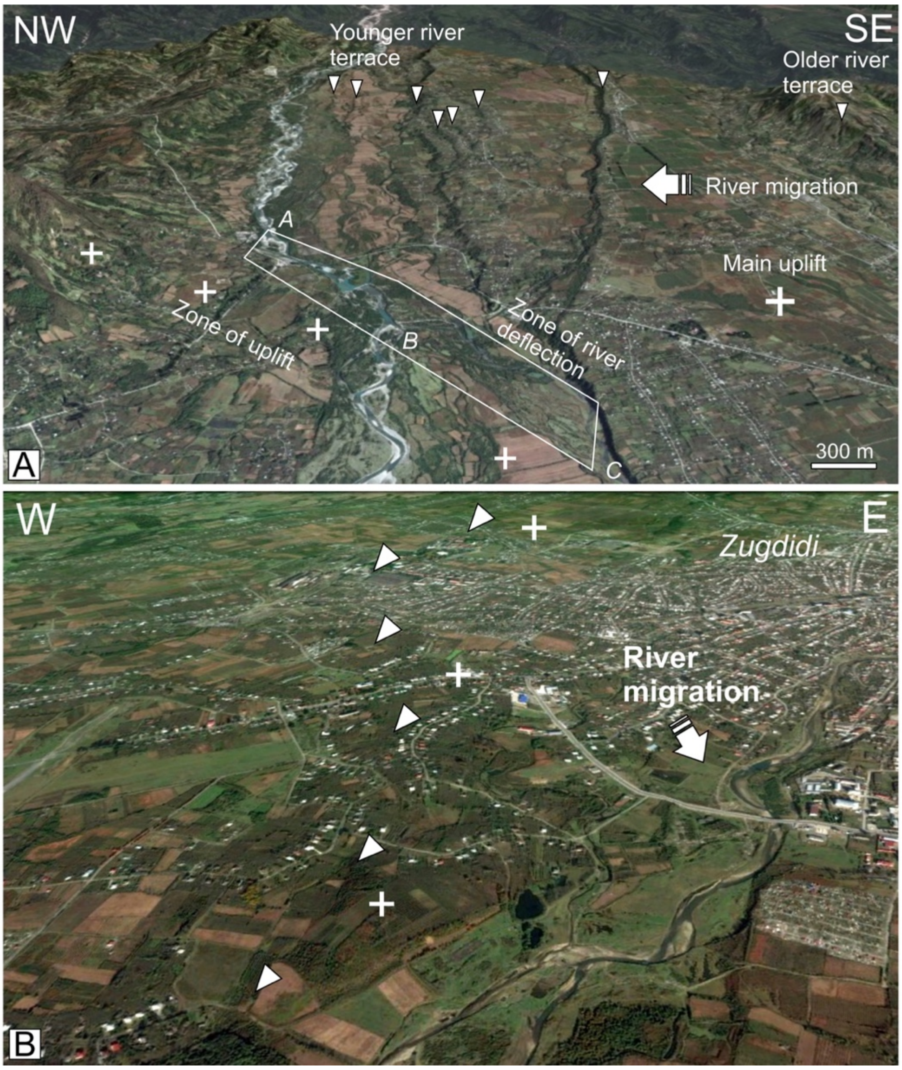

Figure 6. *(A) Westward migration of the northern part of the Enguri River (north of point A) and opposite eastward migration of the southern Enguri segment (south of point B). The white triangles indicate the eight orders of fluvial terraces. The box shows the strip along which the Enguri river has been deviated from point A to point B and also to point C. (B) River migration towards SE induced by an elongated zone of uplift; white triangles indicate the possible fault scarp. (GoogleEarth oblique views, 3x vertical exaggeration). Location in Figure 4.*

feature, as will be discussed later. The relatively uplifted area located NE of this escarpment shows evidence of past river migration towards SE.

Similar evidence is present at several other areas, as for example in Figures 7A and 7B. In these areas there are traces of ancient water courses in the form of abandoned channels or linear sinuous zones of very high humidity visible in infrared satellite images. These ancient water courses are located between topographic highs and the modern river course, indicating past river migration towards SE. All these areas are located along the frontal part of the uplifted Rioni Basin.

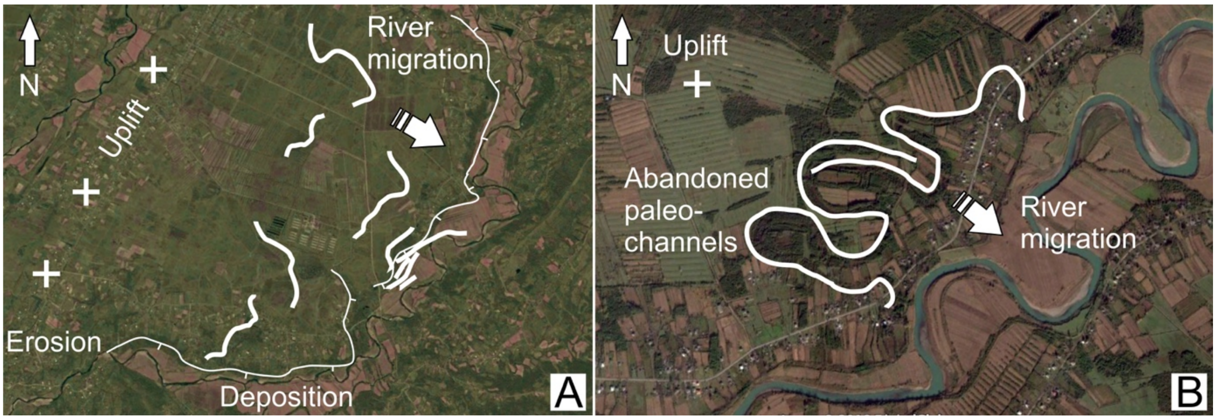

Figure 7. *Migration of rivers induced by differential uplift along the frontal zone of the Rioni Basin uplift. Thick lines represent traces of old river beds as evidenced by differential humidity in infrared satellite images (A) or abandoned channels with still recognizable landforms (B). Thin lines are river terrace escarpments. Crosses indicate zones of uplift. Location n Figure 4.*

In the northern part of the Rioni Basin uplift area, at the foothills of the Greater Caucasus, there is a series of linear features trending WNW-ESE that correspond to outcrops of substrate carbonatic strata with a steep dip angle. In the central part of the uplift area, the morphology is more complex with series of hills with different orientation. They partially correspond to structural highs linked to folds of the substrate or of the Neogene-Quaternary sedimentary deposits, and to old fluvial patterns.

In the central-eastern part of the uplift area, there is an E-W-striking scarp facing north (points A-B in Fig. 4). This scarp cuts the continuity of all the other landforms and interests also the alluvial plane to the east (Fig. 8). Along this segment the Tekhuri river is deflected eastward (B in Fig. 8) and another river is deflected westward (from point A to point A' in Fig. 8). The scarp here is from a few meters high to the east up to 15 m high to the west, as can be appreciated in the detailed GPS topographic profiles that we measured perpendicularly to the scarp (Fig. 9). Further east, the scarp is cut by the Tekhuri river and then there are rare evidence up to the point C of Figure 4 where there is a topographic high of the substrate carbonatic rocks. This outcrop is located south of the possible eastward prosecution of the scarp and shows evidence of overdeepening in the form of an about 20-m-deep gorge excavated by the Abasha river. At the western termination of this scarp, the Ochkhomuri river is deflected westward, whereas an affluent is obliged to run parallel to the scarp. River flow parallel to the scarp may have deepened locally the scarp height, but cannot explain the escarpment formation as a whole. The scarp here, always facing northward, is up to 25 m high. The total length of the scarp is 17.5 km along the segment A-B, and 22 km

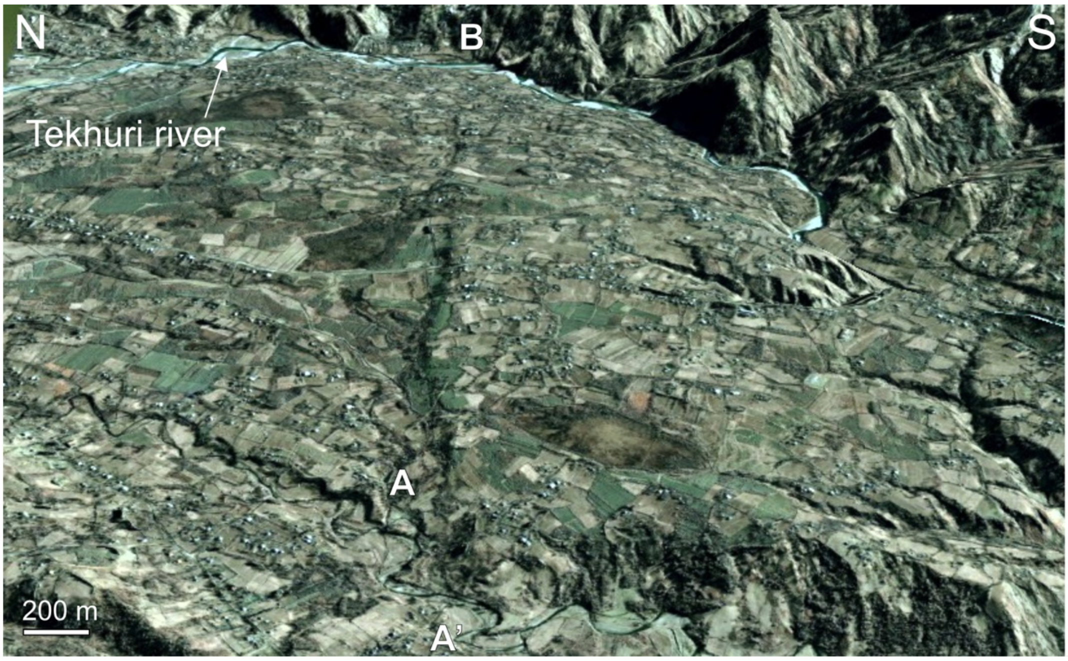

Figure 8. *Oblique view (Google Earth, 3x vertical exaggeration) of the eastern part of the E-W scarp affecting the central-eastern area of the Rioni Basin uplift. The scarp here is cut into the alluvial plane of the Tekhuri river. At point B, the Tekhuri river is deflected eastward, whereas at point A another minor river is deflected westward at point A'.*

if we consider the segment A-C (Fig. 4). In Figure 8 it is also important to observe that the area south of this scarp (right side of the image) is characterised by a slight upward convex profile and overdeepened erosive gullies.

3.2 Structural geology

3.2.1 Main structures

Starting from the northern part of the study area, the substrate of carbonatic rocks of the Greater Caucasus shows a dominant dip towards S and SSW (Fig. 10). The strata dip angle is around 30-50° and then increases southward to 70-90° forming a monocline (Fig. 5C). Some recumbent folds with gentle interlimb angle are present in correspondence of the monocline as well as local overturning. The general strata steepening southward indicates a southern-vergence. No major faults have been detected here in the field, whereas fault planes with some-cm-long fault striae have been detected in a secondary tunnel near the Enguri dam, and will be described in the "Microtectonic data" section.

More to the south, in the Rioni Basin uplift, the substrate carbonatic rocks locally crop out at the foothill of the Greater Caucasus with a sub-vertical dip. Further south

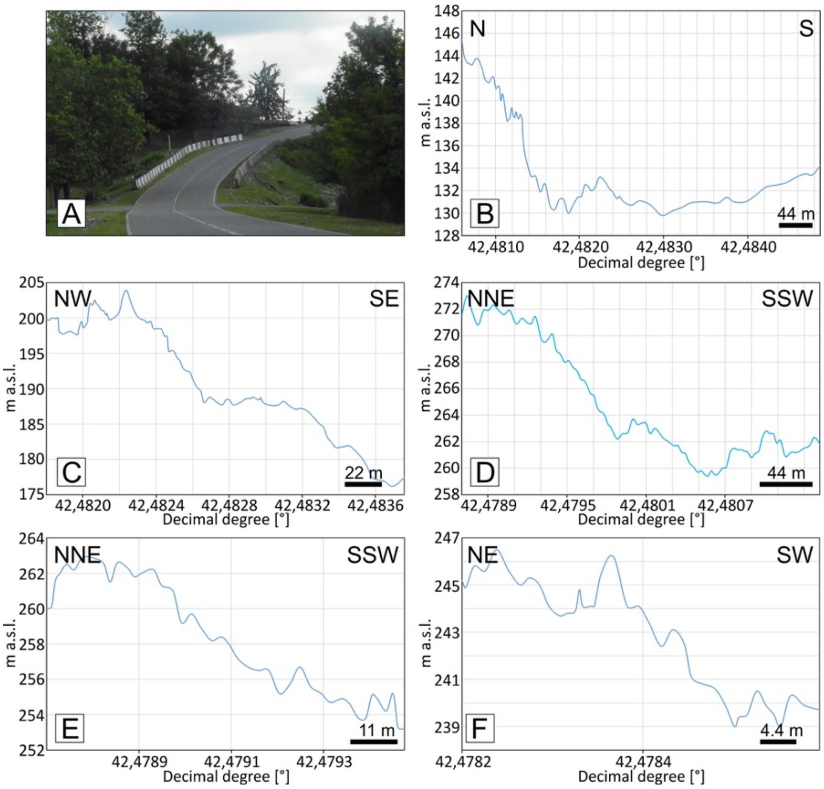

Figure 9. *(A) Photo of the scarp shown in Figure 8. (B-F) Detailed GPS topographic profiles measured perpendicularly to the scarp. The scarp here is from a few meters high to the east up to 15 m high to the west.*

in all the central area of the Rioni Basin uplift, there are several scattered outcrops of Neogene-Quaternary terrigeneous deposits. These are mostly represented by claystones, siltstones and sandstones in the lower stratigraphic part and conglomerates in the upper part. They are arranged in symmetric folds with interlimb angles from gentle to open. The hinge lines trend dominantly N-S to NNE-SSW in the western part and NE-SW to ENE-WSW in the eastern part.

Along the southern and eastern border of the uplift area, there is a series of major folds with substrate rocks of carbonatic and volcanic origin cropping out (Figs. 5D and 10). The topographic culminations of these folds are higher than the remaining topography of the Rioni Basin uplift, and topography becomes flat further south and east. These folds will be described in detail in the following chapter.

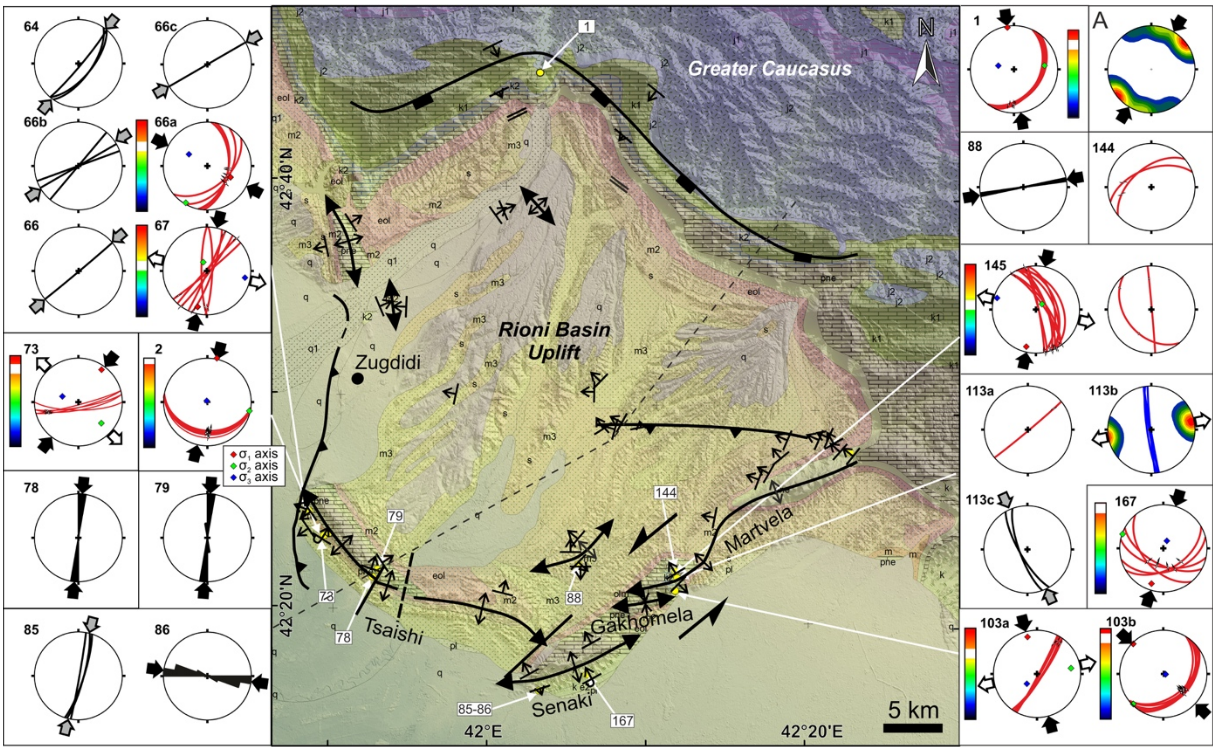

Figure 10. *Map of structures of Rioni Basin uplift area and microtectonic data plotted as lower hemisphere Schmidt's stereograms. In these plots, black arrows give orientation of σ_1 and white arrows of σ_3 if horizontal, calculated with inversion of fault slip data; the white strip in the color bars indicates the tectonic regime (red = reverse, green = strike-slip and blue = normal). Black arrows give σ_1 from tectonic stylolites if associated to rose diagrams showing stylolite peaks. Grey arrows give σ_{Hmax} desumed from extensional joints. Divergent white arrows at site 113b give σ_3 from crystal fibers. Stereogram "A" in the upper right corner gives the average σ_1 and its dispersion from the youngest σ_1 directions surveyed in the whole area. Dashed line shows trace of section of Figure 16.*

3.2.2 Fold geometry

One major fold is located in the southwestern part of the Rioni Basin uplift and is known as Tsaishi fold (Fig. 10). This is an anticline with a more complex structure than previously reported, being characterised by a sub-vertical dip of strata to the southwest, locally overturned, and becoming more gentle towards northeast where strata dip 20-40° to the SW. The axial plane dips about 35° to the NE showing a clear vergence to the SW. The hinge line trends N156° in proximity of the northwestern conical termination of the fold, and N144° along the central and southeastern parts. The fold is 13.2 km long here. More to the east, the continuity of strata is interrupted by two narrow valleys trending NNE-SSW, but the strata dips allow to recognize the same fold that continues for other 16.2 km. The two valleys should coincide with faults as shown by the possible offset of the fold hinge lines. Here the hinge lines trend, from west to east, N100°, N90°, and N126° near the eastern conical termination. As a whole, this fold in plan view has a sinuous "S" shape and a total length of 29.4 km. It involves rocks of Paleocene to Upper Miocene age, but due to the scarcity of outcrops it has not been possible to observe if younger deposits are also folded.

Further east, separated by a NE-trending lineament, there are other three major folds with hinge lines trending ENE-WSW (Fig. 10). They have an en-échelon left-stepping geometry within a corridor trending N45°. The first fold, located to the SW and here named Senaki, has a N78°-trending hinge line in the western part and a N63°-trending hinge line in the eastern part. The strata dip gently towards NNW along the northern limb and steeply towards SSE at the southern limb (e.g. Fig. 5D), with local overturned strata, resulting in a south-vergent anticline (e.g. Fig. 11A). The total length of the outcropping fold is 12.2 km. The fold is affected by some NW-SE-striking right-lateral faults, as in the examples of Figure 12. Deposits of Cretaceous to Middle Miocene age are involved, whereas younger deposits do not crop out here. The deposits here are made both of sedimentary and volcanic rocks. Immediately to the north there is a syncline fold, here named Gakhomela, with a 7.7-km-long hinge line, trending N84°. Further NE, there is another complex major fold, here named Martvili, with a total length of 21.2 km. It has a "S" shape in plan view given by a hinge line trending N67° near the SW termination, N33° in the central part, and N72° towards the NE termination. Strata dip 20-45° to the NW along the northern limb and up to subvertical along the opposite limb, giving rise to an asymmetric,

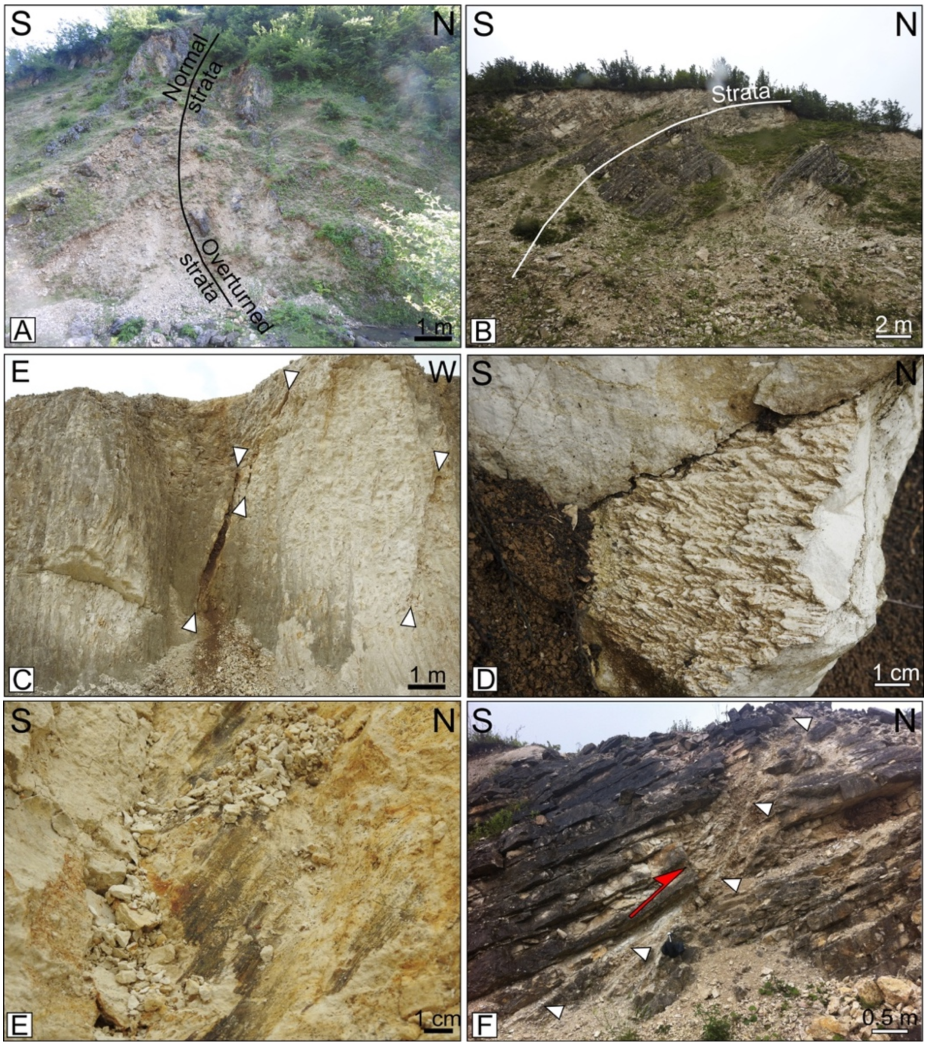

Figure 11. *(A) Overturning of strata at the southern limb of the Senaki fold. (B) Steepening of strata at the southern limb of the Tsaishi fold. (C) Example of the youngest structures at the Tsaishi fold given by N-S-striking extensional fractures. (D) Stylolites giving N-S compression at the Tsaishi fold. (E) Example of striated reverse fault at the southern limb of the Tsaishi fold. (F) Example of backthrust here given by a south-dipping reverse slip plane, found in the central part of the Tsaishi fold.*

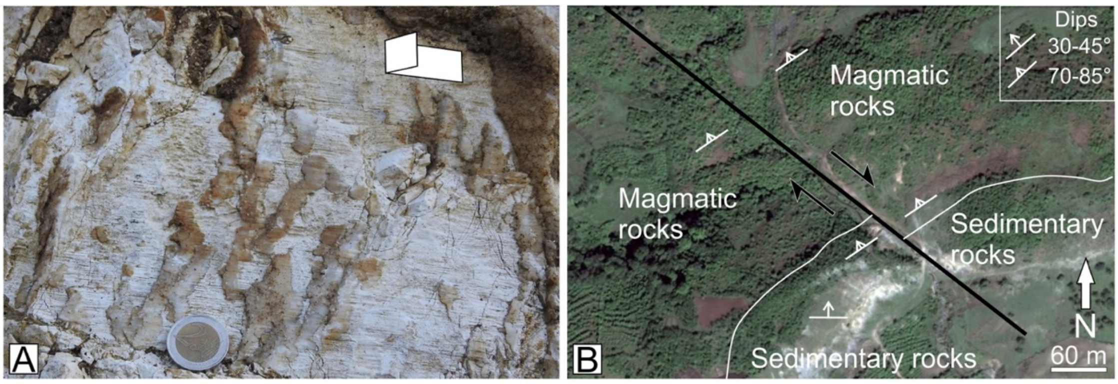

Figure 12. *(A) Example of right-lateral strike-slip fault in carbonatic rocks with accretionary fibers at Senaki fold. (B) Example of NW-striking right-lateral fault affecting the Senaki fold, with offset of the sub-vertical limit between Cretaceous magmatic and sedimentary rocks.*

south-vergent anticline. Deposits of Paleocene to Upper Miocene age are involved, but younger deposits do not crop out here.

The age relationships indicate that all these folds developed after the Upper Miocene, but the scarcity of younger deposits prevent from assessing if these folds are still active based only on stratigraphy.

In the interior of the study area, there are folds affecting the Miocene-Pliocene succession and locally also the Quaternary deposits (Fig. 10). The folds affecting the Neogene succession have limbs with strata dip in the range 10-30° giving rise to gentle, broad synclines and anticlines. In the western part of the study area, strata dips suggest folds with hinge lines trending N-S to NNW-SSE. In the eastern part, hinge lines are WSW-ENE to SW-NE. The folds in the interior of the uplift area, thus, are parallel to sub-parallel to the folds along the borders. It is noteworthy to observe that strata here mostly dip towards WNW to NW. The same strata attitude has been systematically measured along the E-W scarp of Figures 8-9, suggesting that the development and geometry of this scarp is independent form any control of strata attitude.

3.2.3 Microtectonic data

Wherever possible we measured microtectonic data in correspondence of the main structures of the study area (stereograms in Figure 10). Data comprise slickenside fault planes with kinematic indicators, extensional joints, veins with accretionary fibers, and tectonic stylolites. Special attention was given to recognize the order of formation of these structures. Fault planes with tectogliphes have been separated in the field based on their age as resulting from the crosscutting relationships between fault planes of different orientation and between faults and lithostratigraphic units. Faults of the same age have been processed with the SG2PS software (Structural Geology to Post Script Converter - http://www.sg2ps.eu; Sasvári and Baharev, 2014), in order to reconstruct the stress tensor. This software allows paleostress inversion using several methods by Turner (1953), Sprang (1972), Michael (1984), Angelier (1990), Fry (1999), Shan et al. (2004), and Mostafa (2005). In this work we performed Paleostress analyses using the direct inversion method INVD (Angelier, 1990) because this methodology is capable of calculating a misfit vector "*v*" between the measured and calculated shear vector, and of minimizing its length, for at least four different striated faults of the same age.

The results are shown in Table 1 and Figure 10. Table 1 gives also plunge and dip of resulting greatest principal stress (σ_1), intermediate principal stress (σ_2) and least principal stress (σ_3), ratio (R (Φ)) between the differences of the principal stress eigenvalues, (σ_2–σ_3)/(σ_1–σ_3), and Misfit Angle (Av) expressed as the average angle between computed shear stress and slip vector. The orientation of the σ_1 has been analysed also based on the statistical trend of the peaks of tectonic stylolites, whereas the greatest horizontal principal stress (σ_{Hmax}) has been also measured as orientation of vertical extensional joints. The orientation of the σ_3 has been also measured based on the orientation of growth of crystal fibres along veins.

In general, reverse faults and strike-slip faults are equally present at most outcrops. Most reverse fault planes dip southward (e.g. Figs. 11E-F) but the offsets indicate they are minor faults. Notwithstanding, it is important to note that shallow brittle deformation here seems to be associated to penetrative faulting in the form of backthrusts respect to the general southward vergence. Transcurrent faults are mostly given by right-lateral strike-slip motions along vertical planes striking NW-SE to N-S (e.g. Figs. 12A-B). Vertical left-lateral strike-slip faults are also present with dominant NNE-SSW to NE-SW strikes.

In Figure 10 the microtectonic observations are differentiated by data types. The most represented directions of the σ_{Hmax} are in the range N5-40° with the average value at N30° (stereogram A in Fig. 10) as obtained by fault slip data inversion, crystal fibre growth, tectonic stylolites, and extensional joints. Fault slip data and stylolites are consistent with $\sigma_{Hmax} = \sigma_1$. Where more than one deformation phase has been recorded by structures, it resulted in σ_{Hmax} orientation varying apparently with time. As an example, at the northwestern part of the Tsaishi fold the older structures are represented by reverse faults (e.g. Fig. 11E). The oldest age can be attributed based on the fact that all the other structures interrupt the continuity of these reverse faults here, and also by the reverse fault dip angles up to 50° suggesting possible tilting. The reverse faults give a subhorizontal N110° σ_1 (site 66a, Fig. 10). Younger strike-slip faults give a horizontal N20° σ_1 (site 67), followed by the youngest structures, here represented by open fissures that suggest a N40-50° σ_{Hmax} (sites 64, 66b and 66). These data indicate an apparent gradual clockwise rotation of σ_{Hmax} with time. At the central part of the Tsaishi fold, a series of striated backthrusts results in a N10° σ_1 (site 2), consistent with the direction of N5° of the σ_1 based on stylolites a few km to the southeast (sites 78-79).

Near the western termination of the Senaki fold, the older structures are represented by stylolites indicating a N105° σ_1 (site 86), followed by the development of vertical extensional joints that give a N14° σ_{Hmax} (site 85). These data indicate a possible large apparent clockwise rotation of σ_{Hmax} with time. At the central part of the Senaki fold, reverse faults dipping SSW (site 167) give a N18° σ_1.

At the southern flank of the southwestern part of the Martvela anticline, the older structures are represented by reverse faults dipping to the southeast (site 103b) that give a horizontal N135° σ_1. These structures have been followed by the development of NE-SW left-lateral transcurrent faults that give a N169° σ_1 (site 103a), thus resulting again in an apparent clockwise rotation with time. At the northern flank of the same fold, NNW-SSE right-lateral strike-slip faults resulted from a N14° σ_1 (site 145), and crystal fibres give a N85° σ_3 that corresponds to a N175° σ_{Hmax} (site 113b). The age relationships between the latter two sites are not clear. The youngest structures here are extensional joints that give a N160° σ_{Hmax} (site 113c).

Finally, in the northernmost part of the study area in an artificial tunnel near the Enguri dam (site 1), several fault planes show oblique slickenside lineations that give a N175° σ_1.

Table 1. Results of paleostress calculation.

Site	Lat (dd°)	Lon (dd°)	N. of data	σ_1 (plg/dip)	σ_2 (plg/dip)	σ_3 (plg/dip)	R (ϕ)	Av Misfit Angle	Tectonic regime
2	42.392	41.827	6	013/00	103/00	207/90	0.483	2.5	PURE COMPRESSIVE
66a	42.409	41.804	5	118/39	209/01	300/51	0.094	5.7	TRANSPRESSIVE
67	42.408	41.805	7	193/13	338/74	101/09	0.322	13.3	PURE STRIKE SLIP
73	42.390	41.822	6	43/17	141/25	283/59	0.645	2.1	PURE COMPRESSIVE
1	42.757	42.0340	6	352/07	085/29	250/60	0.519	1.4	PURE COMPRESSIVE
145	42.371	42.192	10	193/11	058/75	285/10	0.337	3.5	PURE STRIKE SLIP
167	42,289	42.102	6	197/13	288/04	033/76	0.874	4.6	RADIAL COMPRESSIVE
103a	42.356	42.193	5	346/17	083/21	221/63	0.169	2.1	TRANSPRESSIVE
103b	42.356	42.193	7	314/05	224/01	125/85	0.741	1.7	PURE COMPRESSIVE

Ratio (R (Φ)) between the differences of the principal stress eigenvalues, $(\sigma2-\sigma3)/(\sigma1-\sigma3)$; Av Misfit Angle = average angle between computed shear stress and slip vector.

3.3 Seismicity

The seismicity is portrayed in Figure 13 showing data from both the historical (before 1900 AD) and instrumental catalogue. The Intensity of historical earthquakes ranges up to 9 (MSK scale) (Varazanashvili et al., 2011). The M_W of instrumental events is in the 2 to 5.3 range.

The strongest seismic events in the investigated area during the instrumental period are: Samegrelo-Svaneti, 1930 (M_W = 5.3); Menji, 1941 (M_W = 5.2); Western Georgia, 1948 (M_W = 5.0); Gegechkori, 1957 (M_W = 5.3); Achigvari, 1958 (M_W = 5.2); Rechkhi, 1979 (M_W = 5.0). It should be noted that the epicenters are mostly located along the northwestern and southeastern sides of the uplift area. In the southeastern part, a cluster of earthquakes with a NE-SW trend can be recognized; this cluster coincides with the zone of en-échelon folds previously described. The cluster along the northwestern part of the uplift area is represented by the epicenters of the December, 1979 Rechkhi earthquake swarm, made of foreshocks, aftershocks and two main events of M_W 4.9 and 5.0. The earthquake depths were between 2 - 5 km. These earthquakes occurred in the area of Gali water reservoir (belonging to the Enguri hydroelectrical scheme) in coincidence with the filling of this reservoir and of Enguri reservoir. It is important to note that the distance between these reservoirs and the earthquakes was at minimum of 19 km, and the seismic activity of this area is still ongoing. For example, in July, 2010 an earthquake with M_W = 4.9 occurred in the same area. It is thus highly questionable that this swarm was originated by reservoir infilling. In fact, high seismicity linked to tectonic stresses is often manifested (approximately 20 yr period) as earthquake swarms in the area. For example, in June-July, 1941 there were earthquakes swarms with main shocks of M_W = 5.0, M_W = 5.0 and M_W = 5.2). In January, 1957 there was also the large Gegechkori earthquake swarm, which comprised three main shocks of M_W = 5.2, M_W = 5.2 and M_W = 5.3) and several foreshocks and aftershocks.

Instrumental earthquake depths for the study area are provided in the histogram of Figure 13 showing the number of earthquakes with $M_W \geq 4.4$ vs. their depth for the period 1900-2014. The graph shows also the trend line that was calculated through the moving averaging by step 2. In this map we plotted only those events which have a reliable depth estimation taken from the new Georgian catalogue. Most hypocenters are located at depths from 2 to 19 km, and most of them have originated at depth of 9-10 km.

It is important to underscore that one main historical earthquake (M_W = 6.1, Io = 8-9, MSK) did occur immediately southwest of the Tsaishi anticline (Fig. 13). This seismic event took place on 1614 AD (Tsaishi earthquake, Varazanashvili et al., 2011). This epicenter is located exactly along the trace of the escarpment described previously (Figs. 4 and 10A).

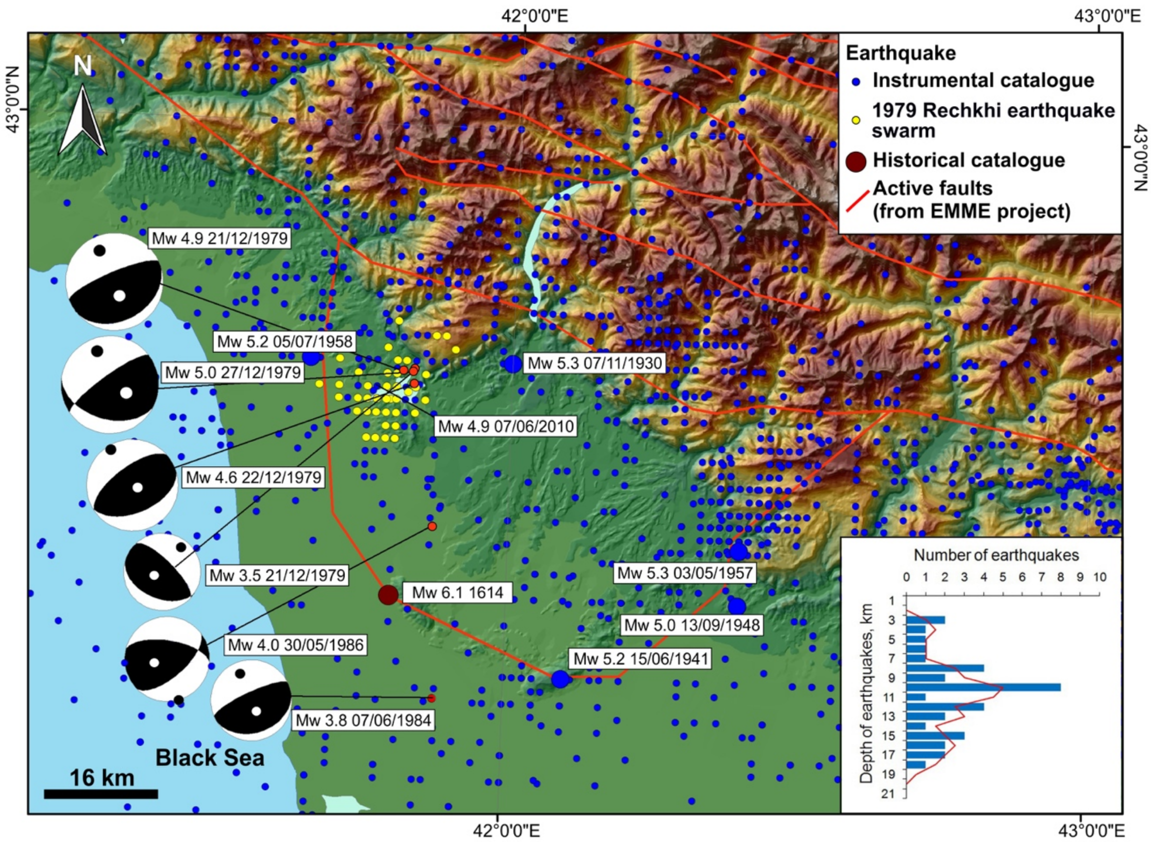

Figure 13. *Distribution of instrumental (yellow and blue circles) and the main historical (brown circle) epicentres in the study area. Earthquake focal mechanism solutions have been computed in the framework of the present work. The histogram shows the number of earthquakes with $M_W \geq 4.4$ vs. their depth for the period 1900-2014 in the study area, together with trend line.*

Some new fault plane solutions for instrumental earthquakes were calculated for the study area (Fig. 13). For determination of the fault planes we used the first motion polarity technique. Only earthquakes for which the number of polarities is equal or more than 8, and azimuthal gaps were less than 180, were selected. All the focal mechanism solutions have a reverse kinematics. The slip fault planes strike NE-SW for five solutions and NW-SE in one case. Following the classification scheme of World Stress Map (Zoback, 1992; Heidbach, 2009) stress regime here is TF (thrust fault).

3.4 Seismic sections

A series of unpublished seismic reflection sections have been here interpreted in order to complete the data surveyed in the field with the geophysical evidence of deeper structures (Figs. 14-15). We obtained three NE-SW trending (A-B, C-D, E-F) and one NW-SE trending (G-H) seismic reflection sections. These sections are concentrated in the southwestern part of the study area, around the Tsaishi fold.

Identification of stratigraphic units at depth of seismic sections was based on outcrop correlations and two deep wells data (box in Fig. 14C). The sections A-B, C-D and E-F reveal in the uppermost part the presence of the south-vergent Tsaishi anticline, of south-vergent thrust faults (F1, F2, F3, F4, F5) and of north-vergent backthrusts (BT1, BT2, BT3).

The Tsaishi anticline is a fault-propagation fold whose front limb is broken by thrust faults. The lower part of these sections are marked by the upper detachment, which correlates to the evaporites of Upper Jurassic age. Above there are units represented by Tertiary, Cretaceous and Upper Jurassic strata. The south-vergent thrust faults, backthrusts, and reactivated and non-reactivated extensional faults in the top section, are the most clear faults observed on the time-migrated seismic data. The middle section between the upper detachment and lower detachment is characterized by blind wedging of the thrust sheets. The bottom section below the lower detachment zone is

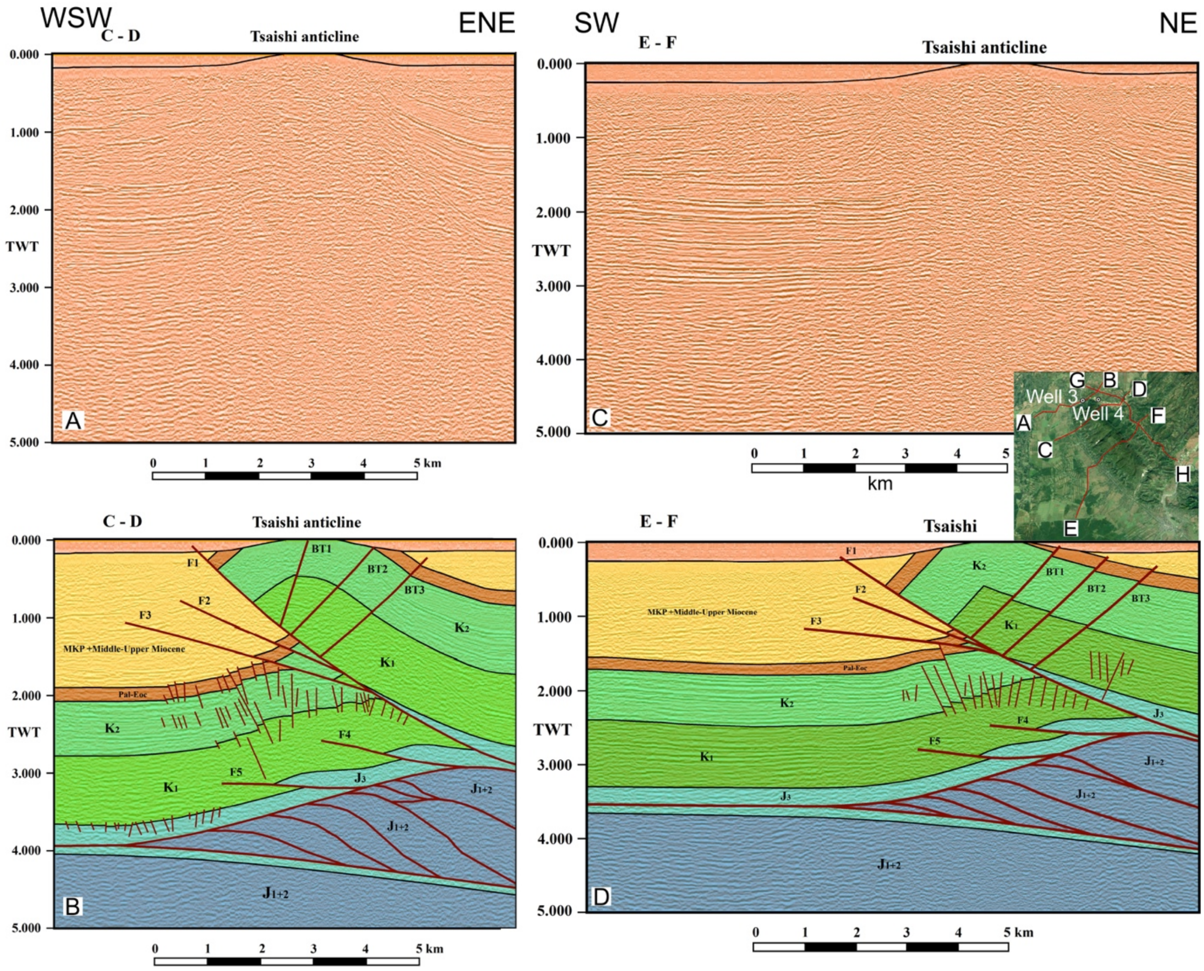

Figure 14. *(A) Uninterpreted and (B) interpreted seismic reflection profiles C-D, and (C) uninterpreted and (D) interpreted seismic reflection profiles E-F. Location in box. Abbreviations: J1+2 Lower and Middle Jurassic; J3 Upper Jurassic; K1 Lower Cretaceous; K2 Upper Cretaceous; Pal-Eoc Paleocene-Eocene; MKP Maikopian (Oligocene-Lower Miocene).*

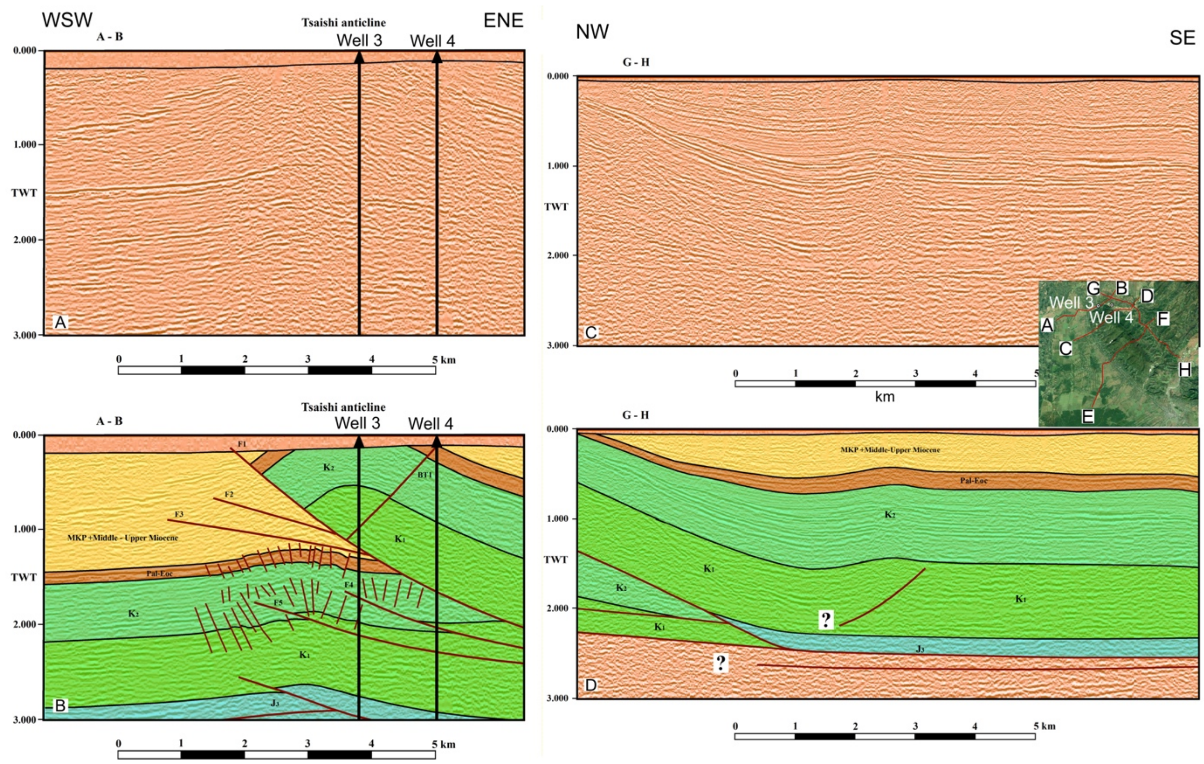

Figure 15. *(A) Uninterpreted and (B) interpreted seismic reflection profiles A-B, and (C) uninterpreted and (D) interpreted seismic reflection profiles G-H. Location in box. Abbreviations: J1+2 Lower and Middle Jurassic; J3 Upper Jurassic; K1 Lower Cretaceous; K2 Upper Cretaceous; Pal-Eoc Paleocene-Eocene; MKP Maikopian (Oligocene-Lower Miocene).*

autochthonous. In the underlying duplex, the thrusts flatten upward into the detachment zone, forming the wedge-shaped triangle zone geometry (Figs. 14B and 14D). South-vergent duplexes involve Middle-Lower Jurassic strata. All the seismic sections suggest that the Rioni Basin tectonics is of thin-skinned type.

4 Discussion

4.1 Geometry of main structures

The study area is limited to the north by a wide asymmetric fold with a gentle-dipping limb strata to the north, and steep-dipping strata to the south, locally verticalized. This structure is morphologically represented by the southern front of the Greater Caucasus where the average altitude drops from 1500-2000 m a.s.l. to the 200-300 m a.s.l. of the Rioni Basin. Our field investigations did not allow to recognize main outcropping active faults along this part of the Caucasus front. Although we admit that the area is heavily covered by forests and of difficult access, the outcrops here do not show any major fault. The only evidence of faulting has been seen inside the artificial tunnel near the Enguri dam. Here microtectonic observations indicate the presence of left-lateral oblique faults dipping N120° (site 1 in Fig. 10). Our field data collected at the Enguri dam zone suggest that this structure here is the effect of a process of fault-propagation folding (A in Fig. 16). A distinctive marker of fault-propagation folds, in fact, is the asymmetric fold profile characterized by a steeply dipping to overturned forelimb and a gently-dipping backlimb. Fault slip progressively decreases along the low-angle propagating ramp, terminating upsection in a blind tip with shortening accomplished by folding (Williams and Chapman, 1983; Suppe and Medwedeff, 1990; Mitra, 1990). This model is consistent with the verticalized strata observed in the field at the forelimb.

On the contrary, fault-bend folds are formed by the passive accommodation of hangingwall strata over a thrust fault that changes dip angle (B in Fig. 16) (Suppe, 1983; McClay, 2011). The distinctive geometry of a fault-bend fold is the more symmetric hangingwall fold profile characterized by a broad anticline with gently-dipping forelimb and backlimb.

Combining the field data with our seismic sections and with those published in Banks et al. (1997), we have reconstructed the structural crustal section of Figure 16. In the northern part of this section, the outcropping strata are arranged into the asymmetric south-vergent fold, interpreted as a fault-propagation fold; this is consistent

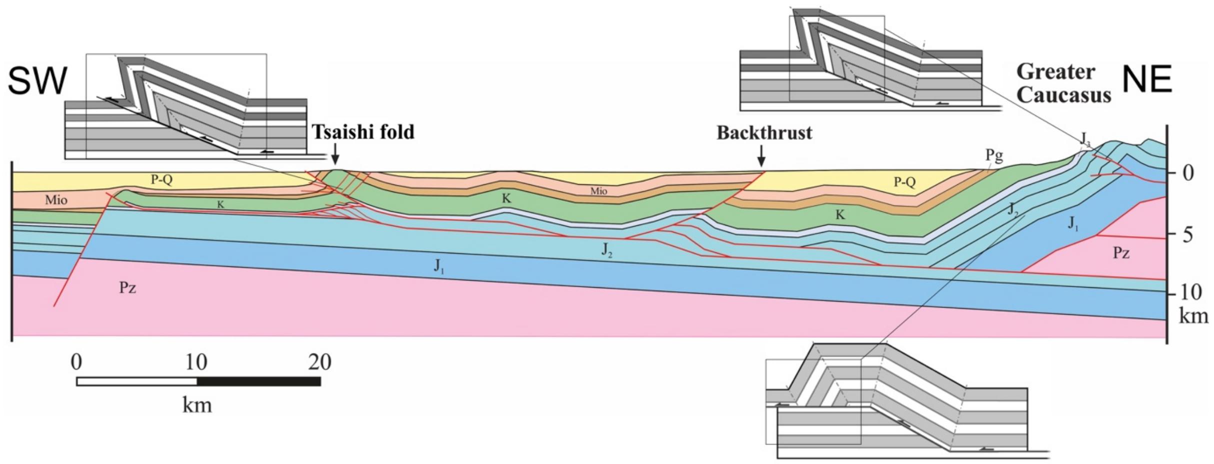

Figure 16*. Structural crustal section obtained by combining our field data and seismic reflection sections with data published in Banks et al. (1997). Pz Paleozoic, lJ lower Jurassic, mJ middle Jurassic, uJ upper Jurassic, lK lower Cretaceous, uK upper Cretaceous, Pg Paleogene, Sar Sarmatian, P-Q Pliocene-Quaternary. Schematic geometric model of (A) a fault-propagation fold (modified after Suppe and Medwedeff, 1990), and (B) a fault-bend fold (modified after Suppe, 1983). The fault-bend fold is characterized by a relative symmetry between the forelimb and backlimb, whereas the fault-propagation fold has a steep to overturned strata in the forelimb. (C) Shows a fault-propagation fold with the thrust reaching the surface. Section trace in Figure 10.*

with a shallow reverse fault interpreted by seismic sections. At a deeper level, the seismic data of Banks et al. (1997) indicate the presence of a thrust plane below the southern frontal zone of the Greater Caucasus. The fault gently dips northward and is here located at a depth of 5-9 km. The geometry of this deeper part of the frontal structure should correspond to a leading anticline-syncline pair, originated as a fault-bend fold with the main ramp located further north. The involved rocks here are given by Jurassic deposits and Paleozoic units.

More to the south, the tectonic block located above the footwall flat is characterised by the presence of deposits of Cretaceous and Tertiary age. These are slightly deformed consistent with the field data where gentle folds are present in the interior of the Rioni Basin uplift. Based on our field data, this tectonic block is interested by a backthrust dipping southward (Fig. 16). This fault is expressed at the surface by the E-W-striking scarp that offsets the Quaternary deposits, illustrated in Figure 8. As shown also in Figure 10, along this scarp the strata dip toward WNW and thus we can exclude an origin of morphoselection. We have also to exclude that this scarp is the expression of a river terrace since rivers here have always been running perpendicularly to the scarp strike. The rocks that crop out at the footwall block are given by silty and clay deposits of probable Upper Miocene age. The deviation of the rivers, the overdeepening of the hanging wall block surface, the fact that the fault scarp is cut into Miocene-Quaternary deposits, and the presence of earthquake shallow hypocenters south of the scarp, indicate that this is a recent, probably active, backthrust.

Further south, based on seismic data, the tectonic block above the footwall flat is affected by a splay fault dipping north. This is a blind fault connected with a shallow fault-propagation fold. More to the south, our seismic sections show the presence of another splay fault departing from the main thrust. It describes a north dipping ramp that ends immediately southwest of the Tsaishi fold. Our field data indicate that this is an asymmetric fold with steep-dipping forelimb strata and more gentle-dipping backlimb strata. Moreover, the morphological scarp observed west of the town of Zugdidi and immediately southwest of this fold, might represent the emersion of the thrust splay fault. This interpretation is consistent with the aligned morphological scarps facing towards west (illustrated in Figure 4), with the migration of rivers on the hangingwall block as a response to uplift, and to the occurrence of the 1614 Tsaishi earthquake exactly along this structure. This scarp cannot be related to a river terrace since it has a different orientation respect to the rivers and average altitude increases downvalley along the scarp edge. All these data suggest that the Tsaishi fold is a fault-propagation fold with the thrust plane propagated throughout the entire fold rock succession under the western segment of the fold (C in Fig. 16). Under the eastern segment of the Tsaishi fold instead, the thrust tip is still hidden. Below the Tsaishi fold, a local tectonic wedge developed. Finally, further south, the seismic sections indicate the presence of another blind thrust. As a whole, the tectonic units are arranged into an imbricate series of south-vergent thrust slices.

4.2 Tectonic evolution

The Rioni Basin has been the site of marine sedimentation during Tertiary times, followed by continental deposits during the Upper Miocene-Pliocene. These rocks represent a molasse-type deposition in an E-W-elongated depression limited to the north and to the south by the growing Caucasus mountain belts. The presence of past extensional tectonics is demonstrated by the normal faults found in the seismic sections. These faults are limited to the lower part of the sections since they displace deposits of Jurassic to Paleogene age. The normal faults do not cross deposits of Sarmatian age and younger. The deposits of the interval Paleogene–Middle Miocene are condensed to absent beneath the Rioni Basin, reflecting non-deposition and erosion during foreland basin development (Robinson et al., 1996; Banks et al., 1997). The main fill of the Rioni foreland basin is thus late Miocene to Quaternary in age.

All deposits are involved into reverse faults and folds, indicating that inversion tectonics occurred here since the Sarmatian age. The compressional tectonics took place by the development of main north-dipping ramp-and-flat structures, with flat surfaces mostly developed along a detachment level represented by upper Jurassic evaporites (Banks et al., 1997). The folds started to grow as they moved along the ramp-and flat structure, accompanied by the development of minor reverse faults mostly dipping southward. Thus penetrative minor deformation took place in the form of backthrusting. This was followed by the formation of minor transcurrent faults, and locally the strike-slip tectonics nucleated along a few major structures. This is suggested by the presence of the NNE to NE-trending lineaments that offset the frontal folds. Although it has not been possible to directly observe these fault planes, their rectilinear trace in plan view and the presence of several strike-slip minor faults with the same geometry, are consistent with this interpretation. These major transcurrent faults acted also as nucleus for river erosion, allowing the deepening of a few major river beds across the folds. The latest brittle deformations occurred as vertical extensional joints in the shallowest part of the rock succession, whereas at deeper level the main north-dipping thrust propagated towards the surface in the western part of the study area, and a main backthrust developed in the eastern interior of the uplifting area and reached the surface.

The youngest directions of the σ_{Hmax} are quite homogeneous all over the area following a dominant N-S to NNE-SSW trend. This corresponds to σ_1, consistent also with GPS data (Reilinger et al., 1997, 2006; McClusky et al., 2000) and with focal mechanism solutions at regional level (Tsereteli et al., 2016). The paleostress instead are much more complex showing different orientations with time. We suggest that these different orientations do not correspond to changes in the principal stress direction with time, but they are the effect of rotation of the folds (or at least of some portions) under a simple shear regime, similarly to what has been found for example during the development of en-échelon folds in the Algerian Atlas (Ferrari et al., 1990). Our preliminary field data at Rioni Basin uplift suggest a dominant antickockwise sense of rotation of the structures. Although this rotation is consistent with the en-échelon left-stepping geometry of the folds within a left-lateral shear zone, we retain that the existing data are still not enough to generate a definitive conclusion on the sense of transcurrent motions or other processes that can be associated to the rotation of these folds, and more field studies are necessary.

The contraction and uplift amounts are differential with a gradual increase eastward. This is shown by a series of clues: 1) the average topography increases eastward as illustrated in the graph of Figure 4, 2) the valley bottom altitudes increase in the same direction, 3) in general, the main rivers migrated westward as indicated by the asymmetric several orders of river terraces present on the eastern sides of the valleys, 4) the Upper Miocene-Quaternary succession in the interior of the uplift area mostly dips towards WNW as resulting from differential uplift, 5) folds are more developed in the eastern side of the study area, and 6) a major backthrust developed in the eastern part of the area in response to larger contraction here. This differential pattern is consistent with the westward ongoing propagation of the closure of the Transcaucasian depression. East of the study area in fact, the tectonic units of the Greater Caucasus and the Lesser Caucasus came already into contact after the Neogene closure of the intermontane depression.

4.3 Active tectonics and seismic hazard

The presence of folds and faults affecting Quaternary deposits and the diffuse seismicity testify to the presence of active tectonics in the studied area. The presence of several villages and, above all, of the Enguri hydroelectrical plant, pose a serious concern about geo-hazards. The Enguri 271 m-high-dam, the 15-km-long artificial water reservoir, and the associated installations represent the most important facility of the country for energy production.

Although from the point of view of the general geomorphology of the area it appears that the southern front of the Greater Caucasus is the most prominent feature, in reality our data do not suggest the presence of an outcropping major fault here. The main fault responsible for the development of the structural flexure here is given by the north-dipping blind thrust. This thrust allows the southward motions of this sector of the Caucasus and should relieve the major part of the N-S shortening, since along the opposite northern front of the Caucasus no major active faults have been detected (Reilinger et al., 2006; Avagyan et al., 2010; Tsereteli et al., 2016). In correspondence of the Enguri hydroelectrical scheme, the blind thrust is located at a depth of 4-9 km and due to its gentle dip, it maintains a shallow position below all the area of the Rioni Basin uplift; the hypocentre of a possible future earthquake might occur at any place along this thrust and the shallow depth will prevent a dissipation of the seismic energy.

Two possible surface traces of active faults have been detected: one is located along the western border of the uplift area and passes nearby the Zugdidi town (Fig. 10). This fault has been imaged also on the seismic reflection sections and represents the emersion of the main thrust in the form of a splay fault (Fig. 15). This fault should be responsible for the 1614 Tsaishi earthquake that destroyed the nearby villages. Anyway, the seismic sections indicate the presence of a further thrust slice located more to the south, which represents the real frontal reverse fault of the embricated system.

The other surface fault trace corresponds to the E-W-striking backthrust; also this slip plane is shallow because it should be connected with the main thrust plane. An earthquake here might occur with a focal depth in the order of less than 9 km.

The shallow depth of the main fault planes, the abundant evidence of active tectonics in the area, and the position of these structures at the front of the contractional system of the Greater Caucasus, point to deserve a special attention to the study of this area from the point of view of seismic hazard and risk assessment.

5 Conclusions

New field geological, geomorphological and structural data have been integrated with seismological data and seismic reflection sections to understand the geometry, kinematics and evolution history of part of the Rioni Basin, located between the Greater and Lesser Caucasus in Georgia.

We confirm that marine and continental deposits of Cretaceous-Neogene age have been locally uplifted since the ending of Miocene. The area of uplift is of 1300 km^2, and Plio-Quaternary river deposits have been uplifted up to 200 m above the surrounding plane. The border of this area has been interested by the development of south-vergent asymmetrical folds and strike-slip faults, as already suggested by Banks et al. (1997) and Philip et al. (1989).

Some of these folds have a left-stepping en-échelon geometry and our new microtectonic data indicate rotation of the greatest principal stress σ_1. We thus suggest simple shear deformation linked with the southward propagation of tectonic blocks respect to the main Greater Caucasus front. In the interior of the uplifted area, there are gentle symmetrical folds and one main recent south-dipping reverse fault, corresponding to a backthrust.

A series of morphostructural clues, the tilting of some Quaternary strata, the offset of Quaternary alluvial deposits, and the presence of crustal seismic activity, indicate that compressional tectonics is still active.

The combination of these data with seismic reflection sections shows that the inversion tectonics took place through a series of north-dipping blind main thrusts along the frontal part of a ramp-and-flat structure that becomes deeper below the Greater Caucasus. Contraction and uplift developed at a higher rate in the eastern part of the study area, consistent with the westward ongoing propagation of the closure of the Transcaucasian depression.

Acknowledgments

We acknowledge suggestions on an earlier version of the manuscript by Gulam Babayev and an anonymous reviewer. This study has been done in the framework of the NATO project SfP G4934 "Georgia Hydropower Security", of the International Lithosphere Program - Task Force II, and of the European Space Agency project n.

32309 “Active tectonics and seismic hazard of southwest Caucasus by remotely-sensed and seismological data” that provided the satellite data (Leader A. Tibaldi). Seismic sections were kindly made available by the State Oil and Gas Agency of Georgia.

REFERENCES

Adamia, Sh., Gujabidze, G., 2004. Geological Map of Georgia, 1:500,000 scale. Georgian Department of Geology, ISTC Project.

Adamia, Sh., Lordkipanidze, M. B., Zakariadze, G. S., 1977. Evolution of an active continental margins exemplified by the alpine history of the Caucasus. Tectonophysics 40, 183-199.

Adamia, Sh., Chkhotua, T., Kekelia, M., Lordkipanidze, M., Shavishvili, I., Zakariadze, G.1981. Tectonics of Caucasus and adjoining regions: implications for the evolution of the Tethys ocean. J. Struct. Geol. 3, 437–447.

Adamia, Sh., Alania, V., Chabukiani, A., Chichua, G., Enukidze, O., Sadradze, N., 2010. Evolution of the Late Cenozoic basins of Georgia (SW Caucasus): a review. In: Sedimentary basin tectonics from the Black Sea and Caucasus to the Arabian Platform (Eds. M. Sosson, N. Kaymakçı, R. Stephenson, F. Bergerat), Geological Society of London, Special Publication, 340, 239-259.

Adamia, Sh., Zakariadze, G., Chkhotua, T., Chabukiani, A., Sadradze, N., Tsereteli, N., Gventsadze, A., 2011a. Geology of the Caucasus: A Review. Turkish Journal of Earth Sciences 20, 489–544.

Adamia, Sh., Alania, V., Chagelishvili, R., Chabukiani, A., Enukidze, O., Jaoshvili, G., Razmadze, A., Sadradze, N., 2011b. Tectonic setting of Georgia (Caucasus). 3rd International Symposium on the Geology of the Black Sea Region 1-10 October 2011, Bucharest, Romania. Abstracts Supplement to GEO-ECO-MARINA 17, 11-13.

Adamia, Sh., Alania, V., Tsereteli, N., Varazanashvili, O., Sadradze, N., Lursmanashvili, N., Gventsadze, A., 2015. Post-Collisional Tectonics and Seismicity of Georgia. In: Tectonic Evolution and Seismicity of south-west Asia. Geological Society of America (GSA) Special Paper (in press).

Alania, V., Chabukiani, A., Chagelishvili, R., Enukidze, O., Gogrichiani, K., Razmadze, A., Tsereteli, N., 2016. Growth structures, piggyback basins and growth strata of Georgian part of Kura foreland fold and thrust belt: implication for Late Alpine kinematic evolution. In Tectonic Evolution of the Eastern Black Sea and Caucasus (eds M. Sosson, R. Stephenson & Sh. Adamia). Geological Society of London, Special Publications no. 428, doi:10.1144/SP428.5.

Albino, I., Cavazza, W., Zattin, M., Okay, A., Adamia, Sh., & Sadradze, N. 2014. Far-field tectonic effects of the Arabia–Eurasia collision and the inception of the North Anatolian Fault system. Geological Magazine 151, 372–79.

Allen, M., Jackson, J., Walker, R., 2004. Late Cenozoic reorganization of the Arabia-Eurasia collision and the comparison of short-term and long-term deformation rates. Tectonics 23, 16, DOI: 10.1029/2003TC001530.

Avagyan A., Sosson M., Karakhanian A., Philip H., Rebai S., Rolland Y., Melkonyan R., Davtyan V., 2010. Recent tectonic stress evolution in the Lesser Caucasus and adjacent regions. In. Sosson, M., Kaymakci, N., Stephenson, R. A., Bergerat, F. & Starostenko, V. (eds), Sedimentary Basin Tectonics from the Black Sea and Caucasus to the Arabian Platform. Geological Society, London, Special Publications 340, 393–408, DOI: 10.1144/SP340.17 0305-8719/10.

Avdeev, B., Niemi N. A., 2011. Rapid Pliocene exhumation of the central Greater Caucasus constrained by low-temperature thermochronometry, Tectonics 30, TC2009, doi:10.1029/2010TC002808.

Banks, C., Robinson, A., Williams, M. 1997. Structure and regional tectonics of the Achara-Trialeti fold belt and the adjacent Rioni and Kartli foreland basins. Republic of Georgia. In Regional and Petroleum geology of the Black Sea and Surrounding Region (ed. A. G. Robinson), pp. 331-36. American Association of Petroleum Geologists Memoir 68.

Cloetingh, S., Spadini, G., Van Wees J. D., Beekman, F., 2003. Thermo-mechanical modelling of the Black Sea Basin (de)formation. Sediment. Geol. 156, 169–184.

Devlin, W. J., Cogswel, J. M., Gaskins, G. M., Isaken, G. H., Picther, D. M., Puls, D. P., Stanely, K. O., and Wall, G. R. T. 1999. South Caspian Basin: Young, cool, and full of promise. GSA Today 9, 7, 1–9.

Dercourt, J., Zonenschain, L. P., Ricou, L. E., Kazmin, V. G., Le Pichon, X., Knipper, A. L., Grandjacquet, C., Sbortshikov, I. M., Geyssant, J., Lepvir, C., Pechersky, D. H., Boulin, J., Sibuet, J. C., Savostin, L. A., Sorokhtin, O., Westphal, M., Bazhenov, M. L., Lauer, J. P., Biju-Duval, B., 1986. Geological evolution of the Tethys belt from the Atlantic to the Pamirs since the Lias. Tectonophysics 123, 241–315.

Ferrari, L., Tibaldi, A., Brizzolara, L., Maffioli, A., 1990. Eocene simple shear and Pliocene pure shear folding in the central-eastern Algerian Atlas. Terra Nova 2, 653-660.

Finetti, I., Bricchi, G., Del Ben, A., Pipan, M., Xuan, Z. 1988. Geophysical study of the Black Sea. Boll. Geofis. Appl. 30, 197–324

Forte, A., Cowgill, E., Bernardin, T., Kreylos, O., Hamann, B. 2010. Late Cenozoic deformation of Kura fold-thrust belt, southern Greater Caucasus. Geological Society of American Bulletin 122, 465-86.

Forte, A., Cowgill, E., Whipple, K. X. 2014. Transition from a singly vergent to doubly vergent wedge in a young orogen: The Greater Caucasus. Tectonics 33, 2077-2101.

Heidbach, O., 2009. Spatial and temporal variability of the contemporary crustal stress pattern of the earth (Doctoral dissertation, Zugl.: Karlsruhe, Univ., Habilitationsschr.).

Jones, R. W., Simmons, M. D., 1997. A Review of the Stratigraphy of Eastern Paratethys (Oligocene-Holocene), With Particular Emphasis on the Black Sea. In Regional and Petroleum geology of the Black Sea and Surrounding Region (ed. A. G. Robinson). American Association of Petroleum Geologists Memoir 68, 39-52.

Kadirov, F.A., Gadirov, A.G., Babayev, G.R., Agayeva, S.T., Mammadov, S.K., Garagezova, N.R., Safarov, R.T., 2013. Seismic zoning of the southern slope of Greater Caucasus from the fractal parameters of earthquakes, stress state and GPS velocities. Izvestiya, Physics of the Solid Earth 49, 4, 554–562 (in Russian).

Khain, V. E., 1974. Structure and main stages in the tectono-magmatic development of the Caucasus: an attempt at geodynamic interpretation. Am. J. Sci. 274, 16–23.

Khriachtchevskaia, O., Stovba, S., Stephenson, R. 2010. Cretaceous-Neogene tectonic evolution of the northern margin of the Black Sea from seismic reflection data and tectonic subsidence analysis. In: Sosson, M., Kaymakci, N., Stephenson, R., Bergerat, F., Starostenko, V. (Eds.), Sedimentary Basin Tectonics from the Black Sea and Caucasus to the Arabian Platform. Geol. Soc. London, Spec. Publ. 340, 137–157.

Koçyiğit, A., Yılmaz, A., Adamia, S., Kuloshvili, S., 2001. Neotectonics of East Anatolia Plateau (Turkey) andLesser Caucasus: Implication for transition from thrustingto strike-slip faulting. Geodinamica Acta 14, 177–195.

Koronovskii, N.V., Demina, L.I., 1999. Collision stage of the evolution of the Caucasian sector of the Alpine fold belt: geodynamics and magmatism. Geotectonics 33, 102–118.

Letouzey, J., Biju-Duval, B., Dorkel, A., Gonnard, R., Kritchev, K., Montadert, L., Sungurlu, O.1977. The Black Sea: a marginal basin; geophysical and geological data. B. Biju-Duval, L. Montadert (Eds.), International Symposium on the Structural History of the Mediterranean Basins, Technip, Paris, 363–376.

McClay, K.R., 2011. Introduction to thrust fault-related folding. In: Thrust Fault-Related Folding (K.R. McClay, J. Shaw and J. Suppe, eds). AAPG Mem. 94, 1–19.

McClusky, S., Balassanian, S., A., Demir, C., Ergintav, S., Georgiev, I., Gurkan. O., Hamburger, M., Hurst, K., Kahle, H., Kastens, K., Kekelidze G., King, R., Kotzev, V., Lenk, O., Mahmoud, S., Mishin, A., Nadariya, M., Ouzounis, A., Paradisssis, D., Peter, Y., Prilepin, M, Reilinger R., Sanli, I., Seeger, H., Tealeb, A., Toksoz, M.N., Veis, G., 2000. Global Positioning System constraints on plate kinematics and dynamics in the eastern Mediterranean and Caucasus. Journal of Geophysical Research: Solid Earth 105(B3), 5695-5719.

McQuarrie, N., Stock, J. M., Verdel, C., Wernicke, B. P., 2003. Cenozoic evolution of Neotethys and implications for the causes of plate motions. Geophysical Research Letter 30, doi:10.1029/2003GL017992.

Mitra, S., 1990. Fault-propagation folds: geometry and kinematic evolution, and hydrocarbon traps. AAPG Bull. 74, 921–945.

Mosar, J., Kangarli, T., Bochud, M., Glasmacher, U. A., Rast, A., Brunet, M., Sosson, M., 2010. Cenozoic–Recent tectonics and uplift in the Greater Caucasus: a perspective from Azerbaijan. In: Sedimentary basin tectonics from the Black Sea and Caucasus to the Arabian Platform (eds. M. Sosson, N. Kaymakçı, R. Stephenson, F. Bergerat), Geological Society of London, Special Publication 340, 261–279.

Okay, A. I., Sengör, A.M.C., Görür, N. 1994. Kinematic history of the opening of the Black Sea and its effect on the surrounding regions. Geology 22, 267–270.

Okay, A. I., Sunal, G., Sherlock, S., Altıner, D., Tüysüz, O., Kylander-Clark, A.R.C., Aygül, M., 2013. Early Cretaceous sedimentation and orogeny on the active margin of Eurasia: southern Central Pontides, Turkey. Tectonics 32, 1247–1271.

Philip, H., Cisternas, A., Gvishiani, A., Gorshkov, A., 1989. The Caucasus: an actual example of the initial stages of continental collision. Tectonophysics 161, 1-21.

Rebai, S., Philip, H., Dorbath, L., Borissoff, B., Haessler, H., Cisternas, A., 1993. Active tectonics in the Lesser Caucasus: coexistence of compressive and extensional structures. Tectonics 12 (5), 1089–1114.

Reilinger, R.E., McClusky, S.C., Oral, M.B., King, R.W., Toksoz, M.N., Barka, A.A., Kinik, I., Lenk, O., Sanli, I., 1997. Global Positioning System measurements of present-day crustal movements in the Arabia-Africa-Eurasia plate collision zone. Journal of Geophysical Research 102 (5), 9983–9999.

Reilinger, R.E., McClusky, S.C., Vernant, P., Lawrence, S., Ergintav, S., Cakmak, R., Ozener, H., Kadirov, F., Guliev, I., Stepanian, R., Nadariya, M., Hahubia, G., Mahmoud, S., Sakr, K., Arrajehi, A., Paradissis, D., Al-Aydrus, A., Prilepin, M., Guseva, T., Evren, E., Dmirotsa, A., Filikov, S. V., Gomez, F., Al-Ghazzi, R. And Karam, G., 2006. GPS constraints on continental deformation in the Africa-Arabia-Eurasia continental collision zone and implications for the dynamics of plate interactions. Journal of Geophysical Research 111(B5), doi: 10.1029/2005JB004051.

Robinson, A. G., Rudat, J. H., Banks, C. J., Wiles, R. L. F., 1996. Petroleum geology of the Black Sea. Marine and Petroleum Geology 13, 195–223.

Spadini, G., Robinson, A., Cloeting, S. 1996. Western v. eastern Black Sea tectonic evolution: pre-rift lithosphere controls on basin formation. Tectonophysics 266, 139–154.

Sosson, M., Rolland, Y., Danelian, T., Muller, C., Melkonyan, R., Adamia, S., Kangarli, T., Avagyan, A., Galoyan, G., 2010. Subductions, obduction and collision in the Lesser Caucasus (Armenia Azerbaijan, Georgia), new insights. In: Sosson, M., Kaymakci, N., Stephanson, R., Bergarat, F., Starostenko, V. (Eds.), Sedimentary Basin Tectonics from the Black Sea and Caucasus to the Arabian Platform, Geological Society of London Special Publication 340, 329-352.

Sosson, M., Adamia, Sh., Muller, C., Sadradze, N., Rolland, Y., Alania, V., Enukidze, O., Hassig, M., 2013. From Greater to Lesser Caucasus: new insights from surface and subsurface data along a N-S trending transect (Georgia): Thick-skin versus thin-skin tectonics. Darius News 3, 5-7.

Sosson, M., Stephenson, R., Sheremet, Y., Rolland, Y., Adamia, Sh., Melkonian, R., Kangarli, T., Yegorova, T., Avagyan, A., Galoyan, G., Danelian, T., Hässig, M., Meijers, M., Müller, C., Sahakyan, L., Sadradze, N., Alania, V., Enukidze, O., Mosar, J., 2016. The Eastern Black Sea-Caucasus region during Cretaceous: new evidence to constrain its tectonic evolution. Compte-Rendus Geosciences 348, 1, 23-32.

Stephenson, R. A., Schellart., W., 2010. The Black Sea back-arc basin: insights to its origin from geodynamic models of modern analogues. In: Sosson, M., Kaymakci, N., Stephenson, R.A., Bergerat, F., Starostenko, V. (Eds.), Sedimentary Basin Tectonics from the Black Sea and Caucasus to the Arabian Platform. Geol. Soc. London, Spec. Publ. 340, 11–21.

Suppe, J., 1983. Geometry and kinematics of fault-bend folding. Am. J. Sci. 283, 684–721.

Suppe, J., Medwedeff, D.A., 1990. Geometry and kinematics of fault-propagation folding. Eclogae Geol. Helv. 83, 409–454.

Tan, O., Taymaz, T., 2006. Active tectonic of the Caucasus: earthquake source mechanisms and rupture histories obtained from inversion of teleseismic body waves. Geological Society of America, special paper 409, 531-578.

Tsereteli, N., Tibaldi, A., Alania, V., Gventsadse, A., Enukidze, O., Varazanashvili, O., Müller, B. I. R., 2016. Active tectonics of central-western Caucasus, Georgia. Tectonophysics 691, 328–344.

Varazanashvili, O., Tsereteli, N., Tsereteli, E. 2011. Historical earthquakes in Georgia (up to 1900): source analysis and catalogue compilation. Monograph, Pub. Hause MVP, Tbilisi, 39-40.

Vincent, S. J., Allen, M., Ismail-Zadeh, A., Flecker, R., Foland, K., Simmons, M., 2005. Insights from the Talysh of Azerbaijan into the Paleogene evolution of the South Caspian region. Geol. Soc. Am. Bull. 117 (11/12), 1513–1533.

Vincent, S.J., Morton, A.C., Carter, A., Gibbs, S., Teimuraz, G.B., 2007. Oligocene uplift of the WesternGreater Caucasus: An effect of initial Arabia-Eurasia collision. Terra Nova 19, 160–166.

Vincent, S. J., Carter, A., Lavrishchev, V. A., Price, S. P., Barabadze, T. G., Hovius, N., 2011. The exhumation of the western Greater Caucasus: a thermochronometric study. Geological Magazine 148, 1–21.

Westaway, R., 1994. Present-day kinematics of the Middle East and eastern Mediterranean. Journal of Geophysical Research 99, 12,071-12,090.

Williams, G., Chapman, T., 1983. Strains developed in the hangingwalls of thrusts due to their slip/propagation rate: a dislocation model. J. Struct. Geol. 5, 563–571.

Yegorova, T., Gobarenko, E., 2010. Structure of the Earth's crust and upper mantle of the West- and East-Black Sea Basins revealed from geophysical data and its tectonic implications. M. Sosson, N. Kaymakci, R.A. Stephenson, F. Bergerat, V. Starostenko (Eds.), Geol. Soc. of London, Spec. Publ. 340, 23–42.

Zakariadze, G., Dilek, Y., Adamia, S., Oberhansli, R., Karpenko, S., Bazylev, B., Soloveva, N., 2007. Geochemistry and geochronology of the Neoproterozoic Pan-African Transcaucasian Massif (Republic of Georgia) and implications for island-arc evolution of the late Precambrian Arabian–Nubian Shield. Gondwana Research 11, 92–108.

Zobak, M. L., 1992. First- and second-order patterns of stress in the lithosphere: The World Stress Map Project. Journal of Geophysical Research 97 B8, 11,703-11,728.

Zonenshain, L. P., Le Pichon, X., 1986. Deep basins of the Black Sea and Caspian Sea as remnants of Mesozoic back-arc basins. Tectonophysics 123, 181–211.